BSGF - Earth Sciences Bulletin 2021, 192, 49

https://doi.org/10.1051/bsgf/2021044

Available online at:
www.bsgf.fr

Special Issue Orogen lifecycle: learnings and perspectives from Pyrénées, Western Mediterranean and analogues ed. O. Lacombe, S. Tavani, A. Teixell, D. Pedreira and S. Calassou (Guest editors)

OPEN ACCESS

Review of the syn-rift to early post-rift depositional systems of the Cretaceous Mauléon Rift: sedimentary record of continental crust hyperextension and mantle denudation (Western Pyrenees)

Nicolas Saspiturry[1,2,3,*], Benoit Issautier[2], Philippe Razin[1], Simon Andrieu[2], Eric Lasseur[2], Cécile Allanic[2], Olivier Serrano[2], Thierry Baudin[2] and Bryan Cochelin[4]

[1] Bordeaux INP, Université Bordeaux Montaigne, G&E, EA 4592, F-33600 Pessac, France
[2] BRGM-French Geological Survey, 3 Avenue Claude Guillemin, 45100 Orléans, France
[3] Université Rennes, CNRS, Géosciences Rennes – UMR 6118, F-35000 Rennes, France
[4] State Key Laboratory for Mineral Deposits Research, Nanjing University, Nanjing 210093, PR China

Received: 4 March 2021 / Accepted: 29 September 2021 / Publishing online: 20 October 2021

Abstract – The Mauléon Basin, in the northwestern Pyrenean Belt, is related to Early Cretaceous rifting and mantle denudation. Here we review the evolution of depositional systems in the Mauléon Rift Basin during Albian and Cenomanian time. This review includes the lithostratigraphy, regional distribution, boundaries, age and facies sedimentology of the basin's syn-rift formations and their members. We construct paleogeographic maps to elucidate (1) the 3D distribution of sedimentary facies and depositional systems during the Albian and Cenomanian from the Iberian proximal margin to the hyperextended domain and (2) the link between major extensional structures and sedimentation during rifting and mantle denudation. The Mauléon Rift was supplied during most of the Albian by sediments from the Iberian proximal margin. The southern margin had a steep and abrupt topographic boundary related to a northward crustal rollover along the south-dipping Saint-Palais detachment. This feature controlled the deposition of coarse-grained turbidites at the base of the margin that abruptly gave way to low-density turbidites, then deep-basin deposits in the hyperextended domain. During uppermost Albian to Early Cenomanian time, mantle denudation occurred in the eastern Mauléon Basin and the vergence of the detachment systems reversed. Minor debris-flow deposits formed at the foot of fault scarps associated with the newly formed north-dipping detachments. Elsewhere, sediment from deltaic systems to the west in the Saint-Jean-de-Luz area deposited low-density turbidites in the hyperextended domain. During the post-rift stage, the flux of coarse sediment from the detachment footwall gradually declined as deformation waned, and low-density turbidites expanded onto the hyperextended domain from the European Upper Cretaceous carbonate platform. These paleogeographic reconstructions, in addition to offering a synthetic view of the evolution of sedimentary environments during rifting, offer new insight into the post-rifting exhumation of the lower crust and mantle.

Keywords: sedimentary facies / depositional systems / paleogeography / Albian-Cenomanian / Mauléon Basin / hyperextension / palinspastic map / Pyrenees

Résumé – Synthèse des systèmes de dépôts syn-rifts à post-rifts du rift crétacé de Mauléon : enregistrement sédimentaire de la phase d'hyperextension de la croûte continentale et de la dénudation du manteau (Pyrénées Occidentales). Le bassin de Mauléon, localisé dans les Pyrénées nord-occidentales, subit une phase de rifting aboutissant à la dénudation du manteau au cours du Crétacé inférieur. Dans ce travail, nous synthétisons l'évolution des systèmes de dépôts Albien à Cénomanien du bassin de Mauléon. Cette synthèse inclut les lithologies, la répartition régionale, les limites stratigraphiques, les âges et les faciès des différentes formations et membres syn-rifts du bassin de Mauléon. Ces derniers ont été temporellement et spatialement corrélés afin de reconstruire des cartes paléogéographiques offrant une meilleure compréhension: (1) de la distribution 3D des faciès sédimentaires et des systèmes de dépôts de

*Corresponding author: saspiturry.nicolas@gmail.com

l'Albien au Cénomanien entre la marge proximale ibérique et le domaine hyper-aminci du bassin de Mauléon et (2) du lien entre les principales structures extensives et la sédimentation au cours du rifting et de la dénudation du manteau. De l'Albien inférieur à supérieur, le bassin de Mauléon était essentiellement alimenté depuis la marge proximale ibérique. La forte pente topographique de cette marge, est due à un basculement vers le nord provoqué par le détachement à vergence sud de Saint-Palais. Cette géométrie a favorisé des dépôts de conglomérats de bassin profond au pied de la marge ibérique passant de manière brutale à des faciès hémipélagiques du domaine hyper-aminci. De l'Albien terminal au Cénomanien inférieur, la vergence des systèmes de détachements s'inverse. Cette étape finale de structuration du bassin conduit à la dénudation du manteau dans la partie orientale du bassin. Des debris flows mineurs, issus de l'érosion sous-marine du mur des détachements à vergence nord, sédimentent au pied des escarpements de failles. À la même époque, les turbidites de faible densité, se déposent dans le domaine hyper-aminci, alimentées par un système deltaïque de polarité Ouest-Est provenant du domaine occidental de Saint-Jean-de-Luz. Au cours du stade postrift, les flux sédimentaires grossiers provenant des escarpements des détachements diminuent corrélativement avec la diminution du jeu tectonique sur ces accidents tandis que les turbidites de faible densité se déposent dans le domaine hyper-aminci proviennent de la plateforme carbonatée européenne. En plus d'offrir une vision synthétique de l'évolution des milieux sédimentaires lors du rifting, ces reconstructions paléogéographiques apportent de nouvelles réflexions quant à l'évaluation de l'exhumation de la croûte inférieure et du manteau.

Mots clés : faciès sédimentaire / systèmes de dépôts / paléogéographie / Albien-Cénomanien / bassin de Mauléon / hyperextension / carte paléogéographique / Pyrénées

1 Introduction

Our knowledge of passive margins has greatly increased during recent decades, partly due to oil and gas exploration and International Ocean Drilling Program campaigns on the Atlantic hyperextended margins, such as Angola and Brazil (Karner *et al.*, 2003; Contrucci *et al.*, 2004; Karner and Gambôa, 2007; Aslanian *et al.*, 2009; Moulin *et al.*, 2010; Unternehr *et al.*, 2010) or Iberia and Newfoundland (Boillot *et al.*, 1987, 1989; Driscoll *et al.*, 1995; Manatschal *et al.*, 2001; Péron-Pinvidic *et al.*, 2007; Péron-Pinvidic and Manatschal, 2009; Reston, 2009; Pérez-Gussinyé, 2013; Haupert *et al.*, 2016). Similarly, investigations of fossil margins in the Alps (Lemoine *et al.*, 1987; Froitzheim and Manatschal, 1996; Manatschal and Nievergelt, 1997; Manatschal *et al.*, 2006, 2011; Beltrando *et al.*, 2014; Decarlis *et al.*, 2015) have documented major detachment faults, leading to new models that precise the mechanisms responsible for subcontinental mantle denudation and exhumation. Hyperextension processes are known to shape magma-poor margins allowing to define three main structural domains (see Péron-Pinvidic *et al.*, 2013 for a review). The proximal margin is characterized by ~30 km thick continental crust. In this domain, the deposits are mainly continental or shallow marine deltaic systems and carbonate platform as described along the West Iberia margin (Alves *et al.*, 2002, 2009). The necking zone, localized at the transition between the shelf and the deep-basin domain, undergo the deposition of gravity flow deposits (Alves *et al.*, 2006, 2020). This domain is affected by a significant amount of crustal thinning due to the development of listric normal faults and detachments (Péron-Pinvidic *et al.*, 2007, 2013). Indeed, the continental crust thickness of this domain is ranging from 25 to 10 km thick. The hyperextended domain is localized in the most distal part of rifts and passive margins. It is characterized by a continental crust thickness of less than 10 km thick. This domain record the deposition of deep-basin marls whose sedimentation is mainly controlled by decantation mechanisms as well as debris flows deposits reworking the footwall of detachments responsible for sub-continental mantle denudation (Masini *et al.*, 2011, 2012; Alves and Cunha, 2018; Ribes *et al.*, 2019).

The evolution of the concepts relative to the hyperextension of the continental crust brings the scientific community to revise the tectonic evolution of the Bay of Biscay margins and the Pyrenean system during the Early Cretaceous rifting stage (Fig. 1). Indeed, in the 80–90's, the Iberian-Eurasian plate boundary was interpreted as a major transcurrent system responsible for the development of pull-apart basins (Debroas, 1987, 1990). Although this idea was recently taken up to explain the formation of the West Pyrenean Mauléon Basin (Canérot, 2017), the scientific community agrees on the fact that the whole North Pyrenean Rift system had undergone hyperextension of the continental crust and sub-continental mantle denudation at the sea floor during Albian to Cenomanian time (Lagabrielle and Bodinier, 2008; Jammes *et al.*, 2009; Lagabrielle *et al.*, 2010, 2020; Masini *et al.*, 2014; Tugend *et al.*, 2015; Teixell *et al.*, 2016, 2018; Lescoutre *et al.*, 2019, 2021; Saspiturry *et al.*, 2020a, 2021, among others). Most of the hyper-thinning crustal models are based on mature passive continental margins characterized by mantle exhumation at the ocean-continent transition. The Mauléon Basin, localized in the Western Pyrenees (Fig. 1), is an exceptional "laboratory" for the unravelling of the tectono-sedimentary evolution of a highly subsiding, thick, sedimentary, rift that undergo mantle denudation. Indeed, this basin preserved a record of the evolution of the depositional systems during continental crust hyperextension despite the subsequent Pyrenean compression (Fig. 2) (Saspiturry *et al.*, 2019a, 2020b). However, the response of the depositional systems during hyperextension, in terms of their process, facies and 3D distribution, is not well characterized. The aim of this article is to analyze the stratigraphic and sedimentological characteristics of the syn-thinning deposits recording hyperextension of the continental crust. In that connection, this paper presents a review of the Albian-Cenomanian syn-rift to post-rift geological formations and members in the Mauléon Basin.

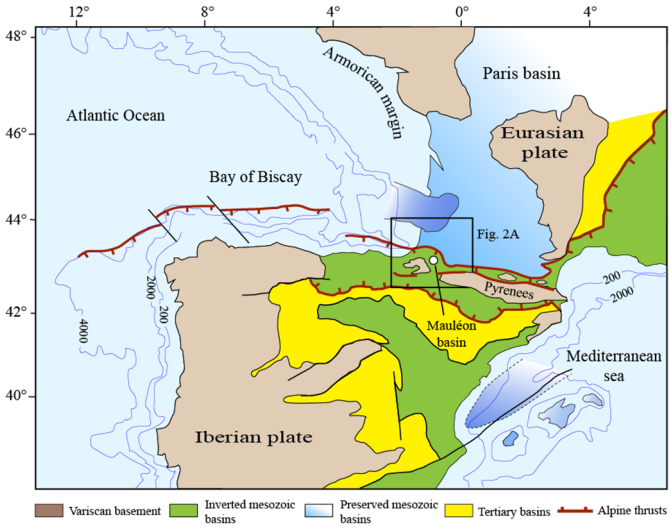

Fig. 1. Simplified structural map of the Cantabrian-Pyrenean orogenic system and adjoining Iberia showing deformed and preserved domains in the Eurasia plate (modified from Lagabrielle *et al.*, 2020).

We propose a synthesis of the evolution of the depositional systems within the three main structural domains of the Mauléon Basin: the proximal margin, the necking zone and the hyperextended domain (Fig. 2C). This approach can be used to reconcile offshore and onshore observations on continental rifted margins. Indeed, first-order relationships can be established between accommodation space creation, depositional system evolution and continental crust thinning to better constrain the mapping of present-day and fossil hyperextended margin structural domains.

2 Geological setting

2.1 Structural units of the Mauléon Basin Iberian Margin

The Pyrenees results from the inversion of Early Cretaceous Rift Basins during the Late Santonian to Miocene (Puigdefàbregas and Souquet, 1986; Olivet, 1996; Saspiturry *et al.*, 2020b). These so-called North Pyrenean Basins developed in an alignment oriented roughly N110° and thus are partly responsible for the current trend of the Pyrenean realm (Souquet *et al.*, 1977). The Pyrenees is composed of three major structural domains named the South Pyrenean Zone, the Axial Zone and the North Pyrenean Zone (Souquet *et al.*, 1975). In the Western Pyrenees, the North Pyrenean Zone corresponds to the closure of the Early Cretaceous Mauléon Rift Basin (Ducasse and Velasque, 1988; Saspiturry *et al.*, 2019a). This basin is currently bordered to the north by the North Pyrenean Frontal Thrust and to the south by the Lakhoura Thrust system (Figs. 2B and 2D; Daignières *et al.*, 1994; Teixell *et al.*, 2016; Saspiturry *et al.*, 2020b).

Using seismic interpretation, gravity inversion, field mapping and crustal-balanced cross-section restoration, Jammes *et al.* (2009), Masini *et al.* (2014), Tugend *et al.* (2015), Saspiturry *et al.* (2020a) and Lescoutre *et al.* (2021) mapped the characteristic domains of hyperextended systems through the Bay of Biscay margins and the inverted Mauléon Basin, *i.e.*, the proximal margin, the necking zone and the hyperextend domain (Fig. 2C).

On the south side of the Mauléon Basin, the Bidarray, Aldudes and Axial Zone structural units have been interpreted by Masini *et al.* (2014) and Tugend *et al.* (2015) as the Albian-Cenomanian proximal margin of the Mauléon Rift Basin (Figs. 2B and 2C). The Bidarray Unit is a singular domain of the Western Pyrenees that represents a N-S trending Permian Rift Basin including an E-W elongated gneiss dome (the Ursuya Unit) that exhumed mid-crustal granulite and migmatite during the Permian (Saspiturry *et al.*, 2019b and references therein). The Permian continental facies of the Bidarray Basin (Lucas, 1985) unconformably overlies the Paleozoic basement and is in turn overlain by a Lower Triassic sequence (the Buntsandstein facies). The Bidarray Unit lacks any Jurassic-Cretaceous sedimentary cover (Fig. 2B). To the south, the Aldudes Unit consists of Ordovician to Carboniferous metasedimentary rocks (Muller and Roger, 1977). To the east, the southern part of the Mauléon Basin is thrusted southward onto the Axial Zone along the Lakhoura-Eaux Chaudes Thrust system (Figs. 2B–2D) (Saspiturry *et al.*, 2020a). The Axial Zone, representing the inverted Iberian proximal margin, is composed of Neoproterozoic to Paleozoic rocks that were highly deformed and metamorphosed late during the Variscan orogeny (Denèle *et al.*, 2014; Cochelin *et al.*, 2017). This basement is unconformably overlain by Upper Cretaceous shallow marine carbonates of the Calcaires des Cañons Formation (Souquet, 1967; Andrieu *et al.*, 2021).

Based on crustal balanced cross-section restoration and field mapping, the Ursuya, Saint-Étienne-de-Baïgorry, Mendibelza, Arbailles and Igountze Units have been interpreted as the inverted Iberian necking zone of the Mauléon Basin (Jammes *et al.*, 2009; Tugend *et al.*, 2015; Saspiturry *et al.*, 2020a; Lescoutre *et al.*, 2021) (Figs. 2B and 1C). The Ursuya Unit is mainly composed of Precambrian to Ordovician metasediments affected by high-temperature, low-pressure metamorphism that reached granulite facies during the Permian (Vielzeuf, 1984; Hart *et al.*, 2016; Vacherat *et al.*, 2017; Lemirre, 2018; Saspiturry *et al.*, 2019b). To the south, the Saint-Étienne-de-Baïgorry Unit is composed of Cretaceous sedimentary breccias (Saint-Étienne-de-Baïgorry and Errozaté Fms.). It is thrusted southward onto the Aldudes domain and is in turn overthrusted by a thick succession of Triassic shale and ophite (igneous rocks) (Fig. 2B). To the southeast, the Mendibelza and Igountze Units are composed of Devonian and Carboniferous low-grade metasediments (Mirouse, 1967) overlain by Albian conglomerate of the Mendibelza Formation (Souquet *et al.*, 1985) and Upper Cretaceous breccias of the Errozaté Formation (Durand-Wackenheim *et al.*, 1981). To the north of the Mendibelza Unit, the Arbailles Unit consists of a narrow syncline in Jurassic to Lower Cretaceous carbonate rocks (Fig. 2B). It is bounded on its northern and southern edges by the North Arbailles and South Arbailles Thrusts (Fig. 2B) (*e.g.*, Saspiturry *et al.*, 2019a).

The domain localized to the north of the North Arbailles Thrust has been interpreted as the inverted hyperextended domain of the Mauléon Basin by Tugend *et al.* (2015) (Figs. 2B and 2C). Based on Vp velocity model, the significant positive Bouguer anomaly associated with the former Mauléon Basin hyperextended domain, mapped by Tugend *et al.* (2015), has

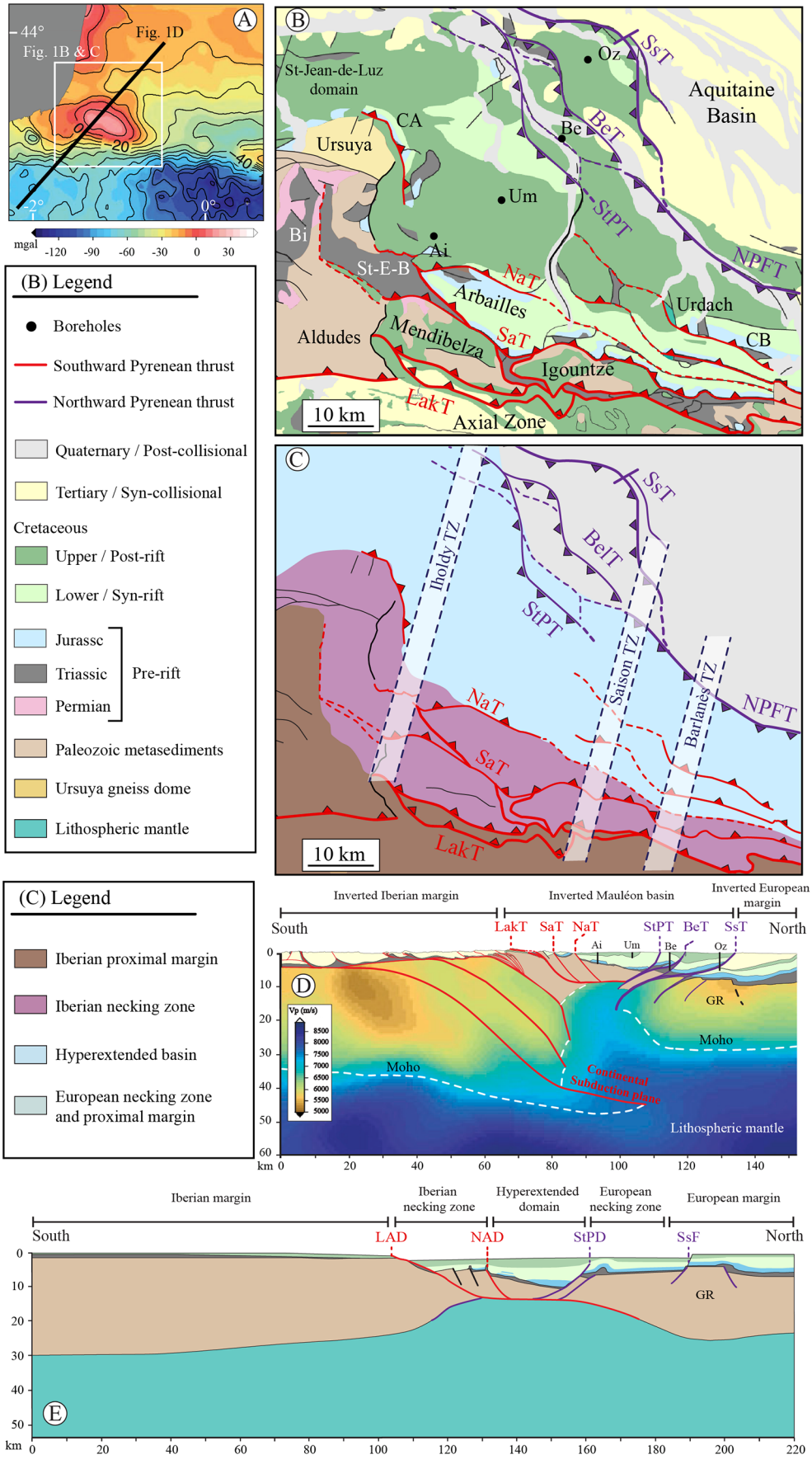
A
44°
Fig. 1B & C
Fig. 1D
2°
0°
mgal
-120 -90 -60 -30 0 30
B
St-Jean-de-Luz domain
CA
Ursuya
Oz
SsT
Aquitaine Basin
Be
BeT
Um
StPT
Bi
Ai
St-E-B
NaT
NPFT
Arbailles
Urdach
Aldudes
Mendibelza
SaT
CB
Igountzé
LakT
Axial Zone
10 km
(B) Legend
Boreholes
Southward Pyrenean thrust
Northward Pyrenean thrust
Quaternary / Post-collisional
Tertiary / Syn-collisional
Cretaceous
Upper / Post-rift
Lower / Syn-rift
Jurassc
Triassic
Permian
Pre-rift
Paleozoic metasediments
Ursuya gneiss dome
Lithospheric mantle
C
Iholdy TZ
SsT
BeIT
StPT
Saison TZ
Barlanès TZ
NPFT
NaT
SaT
LakT
10 km
(C) Legend
Iberian proximal margin
Iberian necking zone
Hyperextended basin
European necking zone and proximal margin
Inverted Iberian margin
Inverted Mauléon basin
Inverted European margin
South
North
LakT SaT NaT StPT BeT SsT
Ai Um Be Oz
D
Vp (m/s)
8500 8000 7500 7000 6500 6000 5500 5000
GR
Moho
Moho
Continental Subduction plane
Lithospheric mantle
km 0 20 40 60 80 100 120 140
Iberian margin
Iberian necking zone
Hyperextended domain
European necking zone
European margin
South
North
LAD
NAD
StPD
SsF
GR
E
km 0 20 40 60 80 100 120 140 160 180 200 220

Fig. 2. (A) Bouguer gravity map of the western part of the Pyrenean Belt displaying a positive anomaly coinciding with the inverted hyperextended domain of the Mauléon Basin (Chevrot *et al.*, 2018). The bold line is the location of the lithospheric profile of Figure 2D. Contour interval, 10 mgal; (B) Geologic map of the Mauléon Basin (modified from Saspiturry *et al.*, 2019b). Major south-vergent thrust faults, shown in red, include the North Arbailles Thrust (NaT), South Arbailles Thrust (SaT), and Lakhoura Thrust (LakT). Major north-vergent thrust faults, shown in purple, include the Saint-Palais Thrust (StPT), Bellevue Thrust (BeT), Sainte-Suzanne Thrust (SsT), and North Pyrenean Frontal Thrust (NPFT). Teeth on upthrown side. St-E-B: Saint-Étienne-de-Baïgorry; Bi: Bidarray Permian Basin. Boreholes: Ai: Ainhice; Be: Bellevue; Oz: Orthez; Um: Uhart-Mixe; CA: Croissant d'Arberoue; CB: Chaînons Béarnais; (C) Structural map showing domains of the Early Cretaceous Mauléon Basin; (D) Lithospheric cross-section of the Mauléon Basin. The upper part corresponds to the crustal-scale balanced cross-section of Saspiturry *et al.* (2020a) and the lower part is derived from the *Vp* model of Wang *et al.* (2016) showing the presence at shallow depth of continental lithospheric mantle inherited from previous Cretaceous hyperextension. GR: Grand Rieu High; (E) Palinspastic restoration, to Santonian time, of the crustal cross-section shown in Figure 2D. Extensional structures: LAD: Lakhoura Detachment; NAD: North Arbailles Detachment; StPD: Saint-Palais Detachment; SsF: Sainte-Suzanne Normal Fault.

thus been interpreted as the presence of subcontinental mantle at shallow depth, ~10 km depth (Figs. 2A and 2D) (Wang *et al.*, 2016). Although this area has undergone Pyrenean compression, crustal-balanced cross-section restoration shows that the continental crust of the central part of the Mauléon Basin is currently characterized by a β factor significantly higher than 2 allowing to properly define this Early Cretaceous Basin as being affected by hyperextension (Saspiturry *et al.*, 2020a). This domain is characterized by the Albian to Lower Cenomanian syn-rift Black Flysch Group (*e.g.*, Souquet *et al.*, 1985). To the east, Early Cretaceous hyperextension ended with mantle denudation from uppermost Albian to mid-Cenomanian time, as recorded by the presence of mantle clasts in breccia of the Urdach Member (Fig. 2B) (Roux, 1983; Duée *et al.*, 1984; Fortané *et al.*, 1986; Debroas *et al.*, 2010; Masini *et al.*, 2014) and by the formation of ophicalcite at the surface of the denudated mantle (Jammes *et al.*, 2009; Lagabrielle *et al.*, 2010, 2019). The syn-rift sediments are overlain by thick Upper Cretaceous calcareous turbidites.

2.2 Mesozoic evolution of the Mauléon Basin

The Mesozoic sedimentary record of the Mauléon Basin begins during the Late Triassic with the Bundtsandstien facies, which corresponds to continental clastics, grading into the Muschelkalk marine carbonate and thence into the Keuper marine evaporite, shale and igneous rocks (Curnelle, 1983; Rossi *et al.*, 2003). This succession represents the large-scale Triassic transgression ending the Hercynian orogenic cycle, and it is related to the opening of the North Atlantic and early rifting of the Neo-Tethys (see Leleu *et al.*, 2016 for a review). The Keuper Unit strongly influences the geometry of Early Cretaceous Rift Basins (Duretz *et al.*, 2019; Lagabrielle *et al.*, 2020; Saspiturry *et al.*, 2021), its thick evaporite sequence acting as a *décollement* layer for thrust development during Eocene time (*e.g.*, Teixell, 1998; Teixell *et al.*, 2016, 2018).

During the Jurassic, the Pyrenean domain was a wide, stable carbonate platform composed of relatively shallow marine carbonates and marls (Peybernès, 1976; Lenoble, 1992; James, 1998; Canérot, 2008). This platform was affected by a major exposure stage between the uppermost Jurassic and earliest Cretaceous, during which a bauxite weathering profile developed (Canérot *et al.*, 1999). From Barremian to earliest Albian time, the future Mauléon Basin was a shallow restricted carbonate platform that graded to inner ramp and bioherm rudist facies in the Aptian (*e.g.*, Canérot, 2008; Saspiturry *et al.*, 2019a), similarly to the adjacent Arzacq Basin (Issautier *et al.*, 2020). These Jurassic to Aptian carbonates and marls constitute the sedimentary cover before hyperextension began.

The development of the Mauléon Rift Basin occurred in the uppermost Aptian to Middle Cenomanian through the development of two diachronous antithetic extensional structures (Fig. 2E) (Saspiturry *et al.*, 2019a, 2020a). The first structure to develop was the south-dipping Saint-Palais extensional detachment, which accommodated thinning of the European margin in Albian time (Fig. 2E). This structure was responsible for the northward tilting of the Iberian margin that led to the northward gliding of the Jurassic-Aptian carbonates and the denudation of the proximal margin Paleozoic basement. Along the Iberian margin, the Paleozoic basement was reworked into the coarse-grained gravity-flow deposits known as the Mendibelza Formation conglomerates (Boirie, 1981). During mid-Cenomanian time, the Saint-Palais detachment system was crosscut by the North-dipping extensional Lakhoura detachment, which acted as the northern boundary of the Iberian necking zone (Fig. 2E). N20° transverse structures, such as the Iholdy, Saison and Barlanès structures (Fig. 2C), also controlled the development of the Mauléon Rift through time (Canérot, 1989, 2008). Their presence is mainly deduced from the positions of syn-rift depocenters and the salt diapirs (Canérot *et al.*, 2005; Debroas *et al.*, 2010). Some of them appear to play a significant role in the basin's structural framework. For instance, the Barlanès structure is punctuated by outcrops where subcontinental mantle (Fabriès *et al.*, 1991, 1998) was reworked into the Albian-Cenomanian Urdach breccias (Roux, 1983; Fortané *et al.*, 1986; Jammes *et al.*, 2009; Lagabrielle *et al.*, 2010; Debroas *et al.*, 2010). This spatial correlation suggests that the Barlanès structure was prominent in the syn-rift denudation of mantle material. Following this Early Cretaceous Rift event, the Mauléon Basin underwent post-rift thermal subsidence and the deposition of distal calcareous turbidites fed from the European carbonate platform (Saspiturry *et al.*, 2019a).

3 Albian and Cenomanian lithostratigraphic units of the Mauléon Basin

Table 1 and the chronostratigraphic chart of Figure 3 summarize the main characteristics of each syn-rift lithostratigraphic unit in the Mauléon Basin: lithology, depositional system, faunal content and age. These formations and members were correlated in order to establish the successive evolution of the depositional systems in the Mauléon Basin from Albian to Cenomanian time. Stratigraphic correlations

Table 1. Inventory of lithostratigraphic formations and members with reference to previous work. Fm., Formation; Mbr., Member.

Antecedents	Lithology	Main Sedimentary deposits	Fossils	Age
Mendibelza Fm. (Lamare, 1946, 1948; Gubler *et al.*, 1947; Magné, 1948; Frey, 1968; Boirie, 1981; Boirie and Souquet, 1982; Fixari, 1984; Souquet *et al.*, 1985; Johnson and Hall, 1989)	Chaotic breccias, unorganized and stratified conglomerates, medium to coarse-grained sandstones with planar laminations and current ripples, massive or laminated sandstone, silty sandstones, dark pelites and olistoliths. The elements are mostly composed of Paleozoic to Triassic meta-sediments.	Deep basin gravity-flow deposits and turbidites	*Douvilleiceras mammillatum*, *Puzosia* sp., *Kossmatella cf. demolyi*, *Beudanticeras*, *Inoceramus concentricus*, *Phylloceras velledae*, *Kossmatella cf. muehlenbecki*, *Hamites* sp., *Anisoceras cf. armatum*,	Early/Late Albian
Saint-Palais Fm. (Casteras *et al.*, 1970, 1971; Boissonnas *et al.*, 1974; Le Pochat *et al.*, 1976; Souquet *et al.*, 1985)	90% of laminated black marls with spicules with 10% of interbedded fine-grained Bouma turbidites with planar lamination and current ripples. The base of the turbidites beds can present a gravel lag with centimetric polygenic clasts of Paleozoic to Triassic meta-sediments.	Hemipelagic deposits and low density turbidites	*Kosmatella* sp. aff. *chabandi*, *Puzozia cf. quenstedti*, *Desmoceras latidorsatum*, *Ptychoceras* sp., *Beudanticeras* sp., *Hoplites* sp., *Inoceramus cf. concentricus*, *Variamussium cf. squamulum*, *Thalmanninella*, *Globigerina waschitensis*, *Aghardiellopsis cretaca*,	Late Aptian/Early Cenomanian
Lanne Mbr. (Fixari, 1984)	Laminated black marls eroded by chaotic breccias with Paleozoic clasts. Unorganized conglomerates with centimetric Paleozoic pebbles and sandstones with planar lamination at their base and current ripple on their top.	Deep basin gravity-flow deposits low density turbidites	No discriminant fauna	Early/Middle Albian
Bustince Fm. (Bouquet, 1986)	Breccias with angular to sub-angular Triassic-Mesozoic clasts, ranging from 1 cm to 10 cm. Olistolithes and sedimentary klippes (up to 15 km^2) of Jurassic to Albian cabonates. Laminated pelites and fine-grained siliciclastic beds.	Deep basin gravity-flow deposits and turbidites	No discriminant fauna	Early/Middle Albian
Flysch de Mixe Fm. (Boissonnas *et al.*, 1974; Le Pochat *et al.*, 1976; Souquet *et al.*, 1985; Razin, 1989; Claude, 1990)	Laminated pelites, sandy turbidites and conglomerates. The coarse sandy turbidites consist of 1 cm up to 20 cm thick beds. Their base is composed of a lag with Paleozoic-Triassic elements. The conglomerates are characterized by a decimetric to rarely metric thickness.	Hemipelagic deposit, low and high density turbidites	*Thalmanninella brotzeni*, *Globigerina waschitensis*, *Rotalipora appenninica*,	Late Albian/Early Cenomanian
Urdach Mbr. (Roux, 1983; Fixari, 1984,	Chaotic breccias with clast size ranging from 3 cm up to 50 cm. Clasts are	Deep basin gravity-flow deposits	No discriminant fauna	Latest Albian/Early Cenomanian

Table 1. (continued).

Antecedents	Lithology	Main Sedimentary deposits	Fossils	Age
Souquet *et al.*, 1985; Debroas *et al.*, 2010)	composed of lherzolites, gneiss, granites, schists and quartzites. This member is also composed of metric olistolithsof the same composition than the breccias.			
Erretzu Mbr. (Fixari, 1984)	Imbricated conglomerates with Paleozoic pebbles and laminated sandstones with a lag of the same composition than the conglomerates. The beds are erosive on laminated dark marls.	Deep basin channelized flow and turbidites	No discriminant fauna	Latest Albian/Early Cenomanian
Saint-Étienne-de-Baïgorry Fm. (Merle, 1974; Le Pochat *et al.*, 1978)	Polygenic breccias with Paleozoic to Albian clasts. Clast a size is ranging from 5 cm up to 1.5 m. Some siliciclastic-limestones are interbedded with the breccias. Albian limestone clasts range from 4 cm to 1 m.	Deep basin gravity-flow deposits	*Hensonina lenticularis*, *Agardhiellopsis cretacea*, *Favusella waschitensis Paraphyllum primaevum*, *Hensonina lenticularis*, *Paraphyllum primaevum*, *Orbitolines*, *Charentia* sp.,	Latest Albian/Early Cenomanian
Errozaté Fm. (Merle, 1974; Le Pochat *et al.*, 1978; Durand-Wackenheim *et al.*, 1981)	Clast-supported breccias with clasts of Paleozoic basement, Upper Triassic ophites and Upper Albian to Santonian Calcaires des Canyons Fm. limestones. The element sizes vary from 1 cm up to 3 m.	Deep basin gravity-flow deposits	*Hensonia lenticularis*, *Charentia* sp., *Charentia cuvillieri*, *Favusella waschitensis*, *Orbitolina conica*, *Orbitolina cuvillieri*, *Trocholina* gr. T *Arabica*, *Praeglobotruncana delrioensis*, *Rotalipora cushmani*, *Praealveolina cushmani*, *Praealveolina cretacea*, *Orbitolina conica*, *Orbitolina paeneconica*, *Orbitolina concava*,	Latest Albian/Santonian
Flysch à silex Fm. (Boissonnas *et al.*, 1974; Le Pochat *et al.*, 1976; Richard, 1986)	Alternating grey marls (metric to decametric thick units), calcareous Bouma sequences and rare breccias. The conglomeratic lag of the turbidites is composed of Paleozoic to Triassic clasts. The calcarenites beds are tabular, and their basal surface is sharp and plane.	Deep basin distal calcareous turbidites	*Thalmanninella* *Rotalipora cushmani* *Globotruncana stephani* *Gumbelina* *Stomiosphera spherical*	Middle/Late Cenomanian
			No discriminant fauna	

Table 1. (continued).

Antecedents	Lithology	Main Sedimentary deposits	Fossils	Age
Bonloc Fm. (Boissonnas *et al.*, 1974; Claude, 1990; Saspiturry, 2019)	Polygenic breccias with angular clasts of granulites, gneiss with garnet, quartzite, pegmatites, Paleozoic meta-sediments. and few clasts of Triassic sandstones and Albian limestones. The matrix is almost absent. The clast size ranges from 5 cm up to 1.5 m. These breccias are interbedded with calcareous turbidites of the Flysch à Silex Fm.	Deep basin gravity-flow deposits		Latest Albian/Late Cenomanian
Hiruraitzeta-Fm. (Saspiturry, 2019)	Breccias interbedded within Tc to Te Bouma calcareous turbidites of the Flysch à Silex Fm. Clasts include Triassic ophites, Devonian-Carboniferous meta-sandstones. Their size is ranging from 1 cm to 8 cm. They are mainly organized in 5 cm to 15 cm thick beds. olistoliths of Triassic ophites.	Deep basin gravity-flow deposits and calcareous turbidites	No discriminant fauna	Latest Albian/Late Cenomanian
Calcaires des Canyons Fm. (Souquet, 1967; Merle, 1974; Le Pochat *et al.*, 1978; Alhamawi, 1992; Andrieu *et al.*, 2021)	Siltstones, sandstones and micro-conglomerates compose the lower part of the formation (Middle to Late Cenomanian). Clasts nature only corresponds to Devonian sediments. This unit grades vertically to Late Cenomanian to Turonian carbonates, consisting in bioclastic grainstones alterning with foraminifers' rich mudstone to packstone and rudists floatstone.	Shallow marine limestones	*Trocholina arabica* *Trocholina* gr. T. *Arabica* *Praealveolina cretacea* *Praealveolina* simplex *Orbitolina conica* *Ovalveolina ovum* *Pseudocyclammina rugosa* *Chrysalidina gradata* *Charentia cuvillieri* *Nezzata* simplex	Early Cenomanian to Santonian

are based on available biostratigraphic markers (Tab. 1) and geologic mapping of lateral and vertical relationships between units.

3.1 Mendibelza Formation

Lithostratigraphy and sedimentary description. Defined by Boirie (1981), Fixari (1984) and Souquet *et al.* (1985), the Mendibelza Formation consists of thick conglomerate deposits with clasts of Paleozoic (Devonian-Carboniferous) and Triassic age (sandstone and igneous rocks). Rare clasts of Albian limestone are visible (Tab. 1). Boirie and Souquet (1982) defined eight sedimentary facies in the Mendibelza Formation: (F1) chaotic breccia (Fig. 4A); (F2) unorganized conglomerate; (F3) stratified and imbricated conglomerate (Fig. 4B); (F4) fining-upward conglomerate interbedded with medium to coarse-grained sandstone with planar laminations at the base and current ripples on top (Fig. 4C); (F5) massive or laminated sandstone with dunes and mega-ripples (Fig. 4B); (F6) silty sandstone (Fig. 4D), (F7) dark pelite (Figs. 4C and 4E), and (F8) olistoliths. Most of the clasts range in size from 10 cm to 1 m, although some reach tens of meters in size.

Regional distribution. The Mendibelza Formation crops out within the Mendibelza and Igountze Units and represents the inverted Iberian necking zone of the Mauléon Rift Basin (Fig. 3). Its thickness can locally reach more than 2000 m (Boirie and Souquet, 1982; Fixari, 1984; Souquet *et al.*, 1985). The thickness of the formation increases gradually from south to north of the Mauléon Basin Iberian necking zone reaching its minimum thickness in the vicinity of the Lakhoura Thrust.

Boundaries. The base of the Mendibelza Formation corresponds to a stratigraphic southward onlap contact onto the Paleozoic metasediments in the Mendibelza and Igountze Units. It is overlain by the onlapping Cenomanian to Santonian Errozaté Formation (Fig. 3).

Age. Stratigraphic correlation indicates an Albian age (Tab. 1).

Depositional system. The F1, F2 and F8 facies are interpreted as debris flow deposits (Boirie, 1981; Fixari, 1984). These facies generally grade upward to highly concentrated flows corresponding to conglomeratic proximal channelized flows of the F3 and F4 facies (Souquet *et al.*, 1985). Channel overflows produced more distal deposits, controlled by turbulent flows, at the mouth of the channel systems (Boirie and Souquet, 1982). These distal deposits make up the F5 and F6 turbiditic facies. The F7 facies corresponds to deposits resulting from decantation mechanisms (Boirie, 1981). Paleocurrent measurements within this formation indicate a direction of supply from SW to NE (Fig. 4F) (Boirie and Souquet, 1982). The depositional system of the Mendibelza Formation has been interpreted as a coarse-grained turbiditic system (Boirie and Souquet, 1982; Souquet *et al.*, 1985) fed by an unpreserved fan deltaic depositional system, localized to the south, that reworked the Paleozoic metasedimentary basement of the Iberian proximal margin (Saspiturry *et al.*, 2019a). The Mendibelza coarse-grained turbiditic system is thus scattered along a steep slope at the transition between the Iberian proximal margin and the Iberian necking zone (Saspiturry *et al.*, 2019a).

3.2 Saint-Palais Formation

Lithostratigraphy and sedimentary description. On the southern part of the Mauléon Basin and the basin depocenter, the Saint-Palais Formation is composed of well-laminated black marls (Fig. 5A) (Souquet *et al.*, 1985). These represent more than 90% of this formation and contain many spicules, *Globigerina*, Rotalidae, ostracodes, and transported bryozoans, coralline red algae and green algae (Dasycladaceae) (Casteras *et al.*, 1970, 1971; Le Pochat *et al.*, 1976). The other 10% of the formation are represented by thin (< 1 m) sandstone beds with planar lamination at their bases and current ripples at their tops. On the European margin, the entire Saint-Palais formation is composed of shallow marine limestones with bryozoans, coralline red algae and green algae (Dasycladaceae). Although these limestones do not crop along the European margin, they have been drilled on several exploration boreholes, north of the Saint-Palais Thrust (Saspiturry *et al.*, 2019b).

Regional distribution. This formation fills the entire hyperextended domain of the Mauléon Basin (Fig. 3) and reaches thicknesses of 1500–4000 m (Souquet *et al.*, 1985; Saspiturry *et al.*, 2019a). The thickness of the formation increases gradually from south to north of the Mauléon Basin hyperextended domain reaching its maximum thickness in the hanging-wall of the Saint-Palais Thrust.

Boundaries. The Saint-Palais Formation unconformably overlies the Jurassic to Albian pre-rift carbonate platform and is overlain by the Flysch de Mixe Formation (Fig. 3).

Age. Stratigraphic markers imply an Albian age (Casteras *et al.*, 1971; Boissonnas *et al.*, 1974; Le Pochat *et al.*, 1976; Souquet *et al.*, 1985; Tab. 1).

Depositional system. The marls have a well-laminated structure interpreted as deep-basin dilute very fine-grained turbidite deposits. Graded sandstone beds within the marls display complete or partial Bouma sequences representing low-density turbidites (Tb–e and Tc–e) (Bouma, 1962). To the south of the Saint-Palais Thrust, the Saint-Palais Formation corresponds to a deep-basin depositional system while to the north of this thrust it is characterized by a shallow marine carbonate platform (Souquet *et al.*, 1985; Saspiturry, 2019). The transported bryozoans, coralline red algae and green algae (Dasycladaceae) present in the Saint-Palais marls are derived from the Saint-Palais limestones developing on the European margin (north of the Saint-Palais Thrust).

3.2.1 Lanne Member

Lithostratigraphy and sedimentary description. The Lanne Member is composed of chaotic clast-supported breccias with erosive bases containing reworked metasediments of the Paleozoic substratum (Fixari, 1984). The uppermost part of this member is composed of unorganized conglomerates with centimeter-sized pebbles of Paleozoic sediments, grading upward to fining-upward sandstone beds with planar lamination at their bases and current ripples on their tops.

Regional distribution. The Lanne Member is exposed north of the Igountze Massif in the transition between the Iberian necking zone and the hyperextended domain (Fig. 3). It locally reaches thicknesses of 300 m (Fixari, 1984).

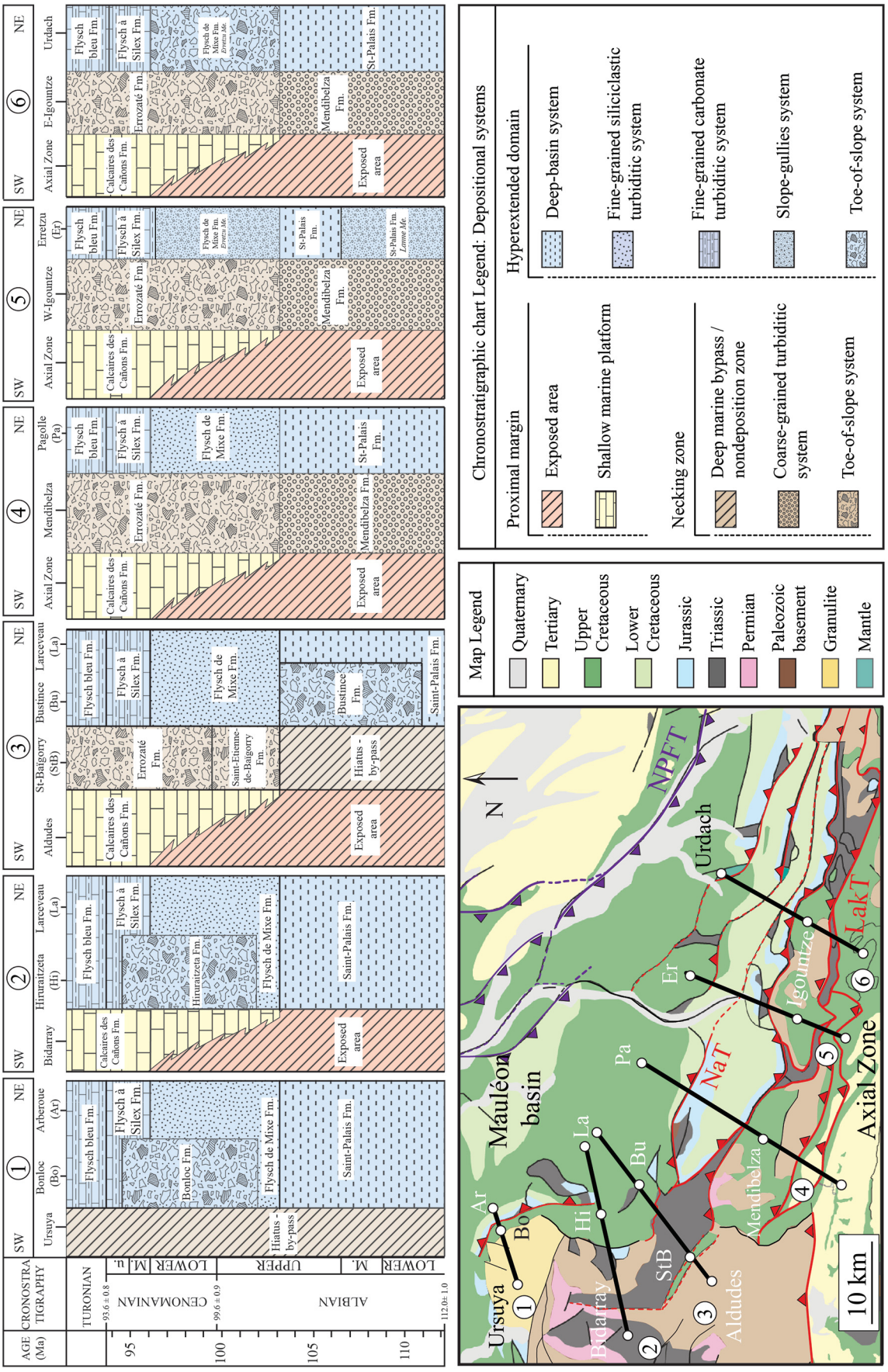

Fig. 3. Albian to Turonian chronostratigraphic chart of the Mauléon Iberian margin and deep basin, with main lithologies, profile locations and depositional systems of the syn-rift formations and members reviewed in this paper.

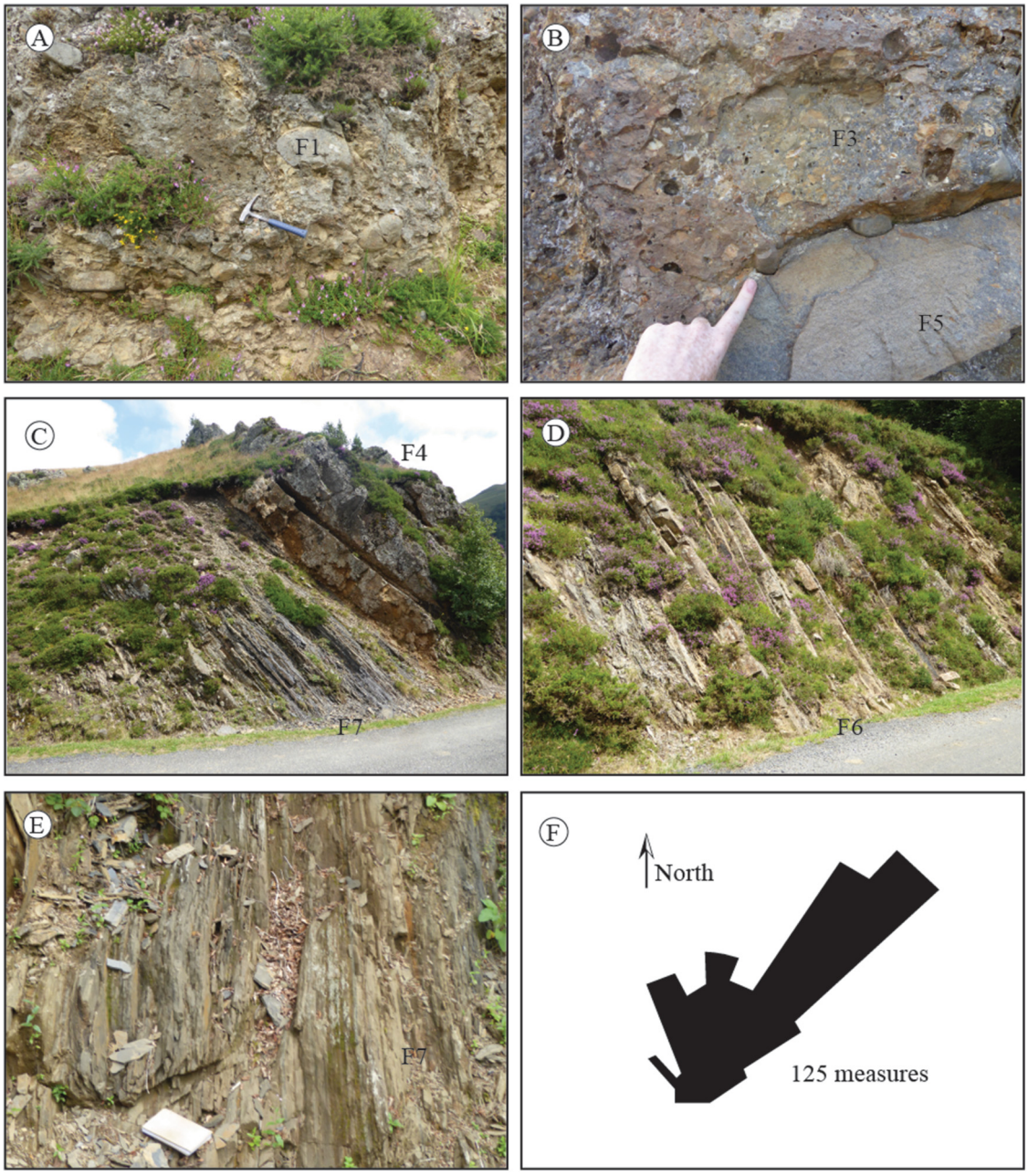

Fig. 4. Features of the Mendibelza Formation corresponding to sedimentary facies of Boirie and Souquet (1982). (A) F1 chaotic breccia with reworked clasts of Paleozoic metasediments; (B) F5 laminated sandstone eroded by F3 stratified and imbricated conglomerate with pebbles and cobbles of Paleozoic metasediments; (C) F7 dark pelite eroded by F4 fining-upward conglomerate interbedded with medium- to coarse-grained sandstone with planar laminations at the base and current ripples on top; (D) F6 silty sandstone; (E) F7 dark pelite; (F) paleocurrent measurements in the Pic des Escaliers area (Boirie, 1981).

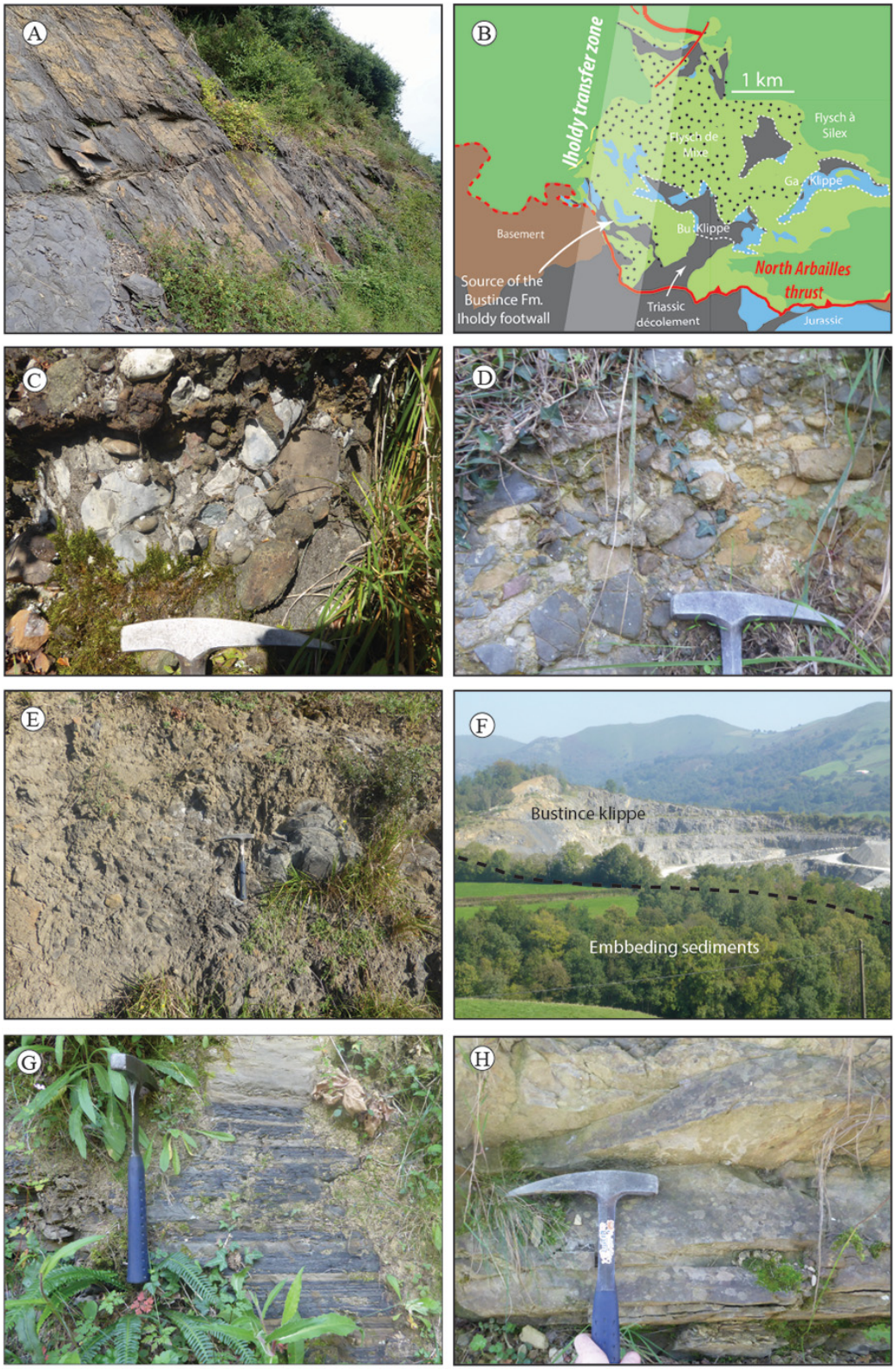

Fig. 5. Field photographs showing (A) outcrop and (B) Geological map of the Bustince Formation. brown: Paleozoic basement, black: Triassic shales and evaporites, blue: pre-rift sedimentary cover, light green: Bustince Formation with pre-rift sedimentary klippes and olistolithes, dark green: post-rift turbidites; (C–G) lithologies of the Bustince Formation; (C) Polygenetic clast-supported breccia with reworked clasts of Upper Triassic igneous rocks, Lower Jurassic limestone and Lower Albian limestone; (D) polygenetic clast-supported breccia with Lower Jurassic and Lower Albian limestone clasts 0.5 to 5 cm in diameter; (E) monogenetic breccia with pebbles and cobbles of Upper Triassic igneous rocks; (F) face of the Bustince-Iriberry quarry in representing a 1.5 km^2 sedimentary klippe of pre-rift limestones; (G) interbedded laminated pelite; (H) interbedded siliciclastic turbidites displaying incomplete Bouma sequences.

Boundaries. The Lanne Member represents the lower part of the Saint-Palais Formation and rests upon Upper Aptian limestones. It is overlain by the Flysch de Mixe Formation (Fig. 3).

Age. Its stratigraphic position between Upper Aptian limestones and the Flysch de Mixe Formation suggests an Early to Middle Albian age (Tab. 1).

Depositional system. The clast-supported breccias may correspond to the Mutti F3 facies: clast-supported debris flow (Mutti, 1977, 1992), and the fining-upward sandstone beds display complete Bouma sequences. Paleocurrent measurements indicate a SE-NW sediment supply direction (Fixari, 1984). The Lanne Member is characteristic of slope-gullies depositional system (Fixari, 1984).

3.3 Bustince Formation

Lithostratigraphy and sedimentary description. The Bustince Formation (Fig. 5B) is composed of clast-supported breccia and more rarely coarse matrix-supported breccias both characterized by angular to subangular clasts ranging in size from 1 to 50 cm. Clasts consist of Jurassic to Early Albian limestone and Late Triassic igneous rocks (Figs. 5C and 5D) and include rare monogenetic igneous rocks breccia (Fig. 5E). The matrix is the same material as the clasts. The breccias appear to include large blocks, olistoliths and several sedimentary klippe up to 1.5 km^2 in size made of Lower or Middle Jurassic to Albian rocks, such as the Bustince and Gamarthe klippes (Fig. 5B) (Bouquet, 1986; Fig. 5F). The contacts between these blocks and the breccias are not visible, which initially led geologists to interpret them as outcrops of pre-rift substratum (Le Pochat *et al.*, 1978). This formation also contains meter-scale olistoliths of Jurassic to Aptian rocks. Beds of laminated pelite (Fig. 5G) and fine-grained sandstone occur within the breccias and between olistoliths.

Regional distribution. The Bustince Formation crops out to the north of the Saint-Étienne-de-Baïgorry area, at the transition between the Iberian necking zone and the hyper-extended domain (Fig. 3). The thickness of this unit is difficult to estimate due to poor exposures but seems to be between 500 and 800 m thick (Bouquet, 1986).

Boundaries. At the base, this formation is delimited by the Arbailles Thrust. It is overlain by a sequence of mixed calcareous and detrital turbidites 15 m to 30 m thick belonging to the Flysch de Mixe Formation (Fig. 3).

Age. The Bustince Formation developed during the Early to Middle Albian: the youngest reworked pebbles are of earliest Albian age, and the formation is conformably overlain by the Flysch de Mixe Formation of Late Albian age (Tab. 1).

Depositional system. The breccias are dominated by clast-supported texture (F3 of Mutti) and more rarely coarse-matrix-supported texture (F2 of Mutti), with poor or no sorting and organization. The intercalated sand beds display incomplete Bouma sequences, suggestive of low-density turbidites deposited on top of the clast-supported breccias. The presence of huge blocks attributable to massive slope failure (olistoliths and sedimentary klippe) indicates the existence of an unstable very steep scarp that enabled efficient transportation of the sedimentary load. These deposits develop within a toe-of-slope depositional system (Bouquet, 1986). At the onset of rifting, the pre-rift sedimentary cover was dismembered during the earliest Albian cover gliding, forming a submarine scarp of pre-rift cover at the foot of the Iholdy transfer zone becoming the source of the Bustince Formation (Saspiturry *et al.*, 2019b). The pre-rift cover was the former cover of the Aldudes basement localized in the Iholdy transfer zone footwall, *i.e.*, to the south-west (Fig. 5B). Thus, the Aldudes area corresponds to the footwall of the salt gliding surface (source area) and the Bustince area to the hanging-wall where the gliding cover accumulated (Saspiturry, 2019).

3.4 Flysch de Mixe Formation

Lithostratigraphy and sedimentary description. The Flysch de Mixe Formation is composed of a very monotonous sequence of alternating black silty marl, subordinate fine to coarse sandstone beds with planar to oblique laminations and conglomerates (Fig. 6A) (Boirie, 1981; Roux, 1983; Fixari, 1984). The black silty marl layers are tens of centimeters to several meters thick and represent 70 to 90% of the formation. The sandstone intervals, representing about 10% of the formation, consist of beds 1 to 20 cm thick with sharp planar bases and wavy upper surfaces. The sandy interval is generally marked at its base by fine-grained conglomerate with rounded, poorly sorted clasts of Paleozoic to Triassic rocks (Razin, 1989). Bioturbations (horizontal worm burrows) are common below this basal surface. Conglomerate facies are rare, forming beds a few centimeters to as much as a meter thick. Clasts are subrounded Paleozoic metasediments. Razin (1989) identified three facies: (1) disorganized sandy matrix-supported conglomerate, (2) clast-supported conglomerate with inverse and normal grading, and (3) fining-upward stratified conglomerate in which the coarse interval gives way abruptly to oblique- or parallel-laminated sandy beds.

Regional distribution. The Flysch de Mixe Formation crops out over the entire Mauléon Basin hyperextended domain (Fig. 3). It can reach 1200 m to 1500 m in thickness.

Boundaries. The base of the Flysch de Mixe Formation is a gradational transition with the Saint-Palais Formation (Fig. 3). It is overlain by the onlapping Middle to Upper Cenomanian Flysch à Silex Formation (Fig. 3).

Age. This formation is dated from Late Albian to Early Cenomanian by ammonites and by its stratigraphic relationship with the overlying Flysch à Silex Formation (Souquet *et al.*, 1985; Razin, 1989; Claude, 1990; Tab. 1).

Depositional system. The laminated pelites correspond to deep-basin deposits which sedimentation is driven by decantation mechanisms. The very thin interbeds of planar to oblique laminated fine to coarse sandstone correspond to small Tb-Tc turbidites. The conglomerates correspond to typical proximal turbidites ranging from debris flow/hyperconcentrate deposits (for the first and second facies, respectively the disorganized conglomerate and the clast-supported conglomerate) to high-density/concentrated turbidity current deposits (for the third facies, fining-upward stratified conglomerate) (sensu Lowe, 1982). The absence of channels or lobes could be the result of the sedimentation of the conglomeratic facies inside the canyon of the slope. The Flysch de Mixe Formation is characteristic of a fine-grained turbiditic depositional system (Razin, 1989). Thirty measured paleocurrents evidence that the sediment supply was

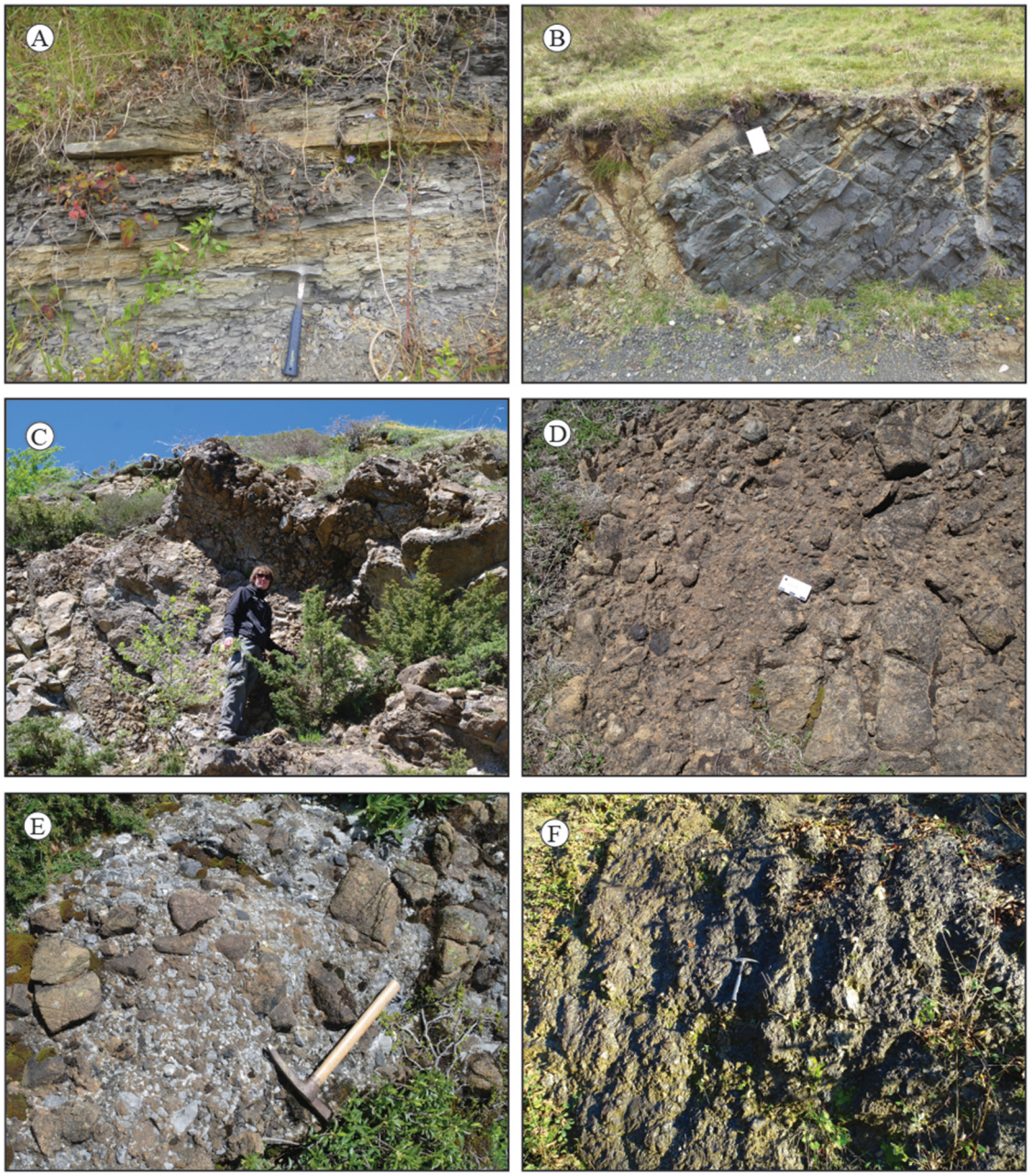

Fig. 6. Field photographs showing (A) micaceous silty marl of the Flysch de Mixe Formation with interbedded fine-grained Bouma-type turbidites; (B) serpentinized mantle rocks of the Urdach Member; (C) typical fresh lherzolite tectonic breccia in the Urdach area; (D) ophicalcite breccia made up of variably serpentinized lherzolite clasts in a calcitic matrix; (E) polymictic lherzolite-marble breccia made up of various types of high-temperature Mesozoic marble; (F) conglomerate of the Erretzu Member made up of centimeter-sized pebbles and subangular clasts.

from west to east in the western part of the Mauléon Basin and north-west to south-east in the Mauléon Basin core (Razin, 1989; Claude, 1990).

3.4.1 Urdach Member

Lithostratigraphy and sedimentary description. The Urdach Member is composed of chaotic breccia with clasts ranging in size from 3 to 50 cm that consist of lherzolite, gneiss, granite, schist and quartzite (Roux, 1983; Fixari, 1984; Duée *et al.*, 1984; Souquet *et al.*, 1985; Fortané *et al.*, 1986; Debroas *et al.*, 2010). The lherzolite clasts are derived from the Urdach mantle outcrop (Fig. 6B). Indeed, lherzolite tectonic breccia is found inside the mantle body along its southern border (Fig. 6C). These monogenic breccias of mantle material are localized along fractures zones. Their texture is magnified by outcrops differential weathering that tends to round the edges of the blocks. The tectonic breccia passes very gradually to a sedimentary breccia that incorporates clasts of Jurassic-Aptian marble with a matrix composed of mantle material. Away from the largest lherzolite body, the Urdach sedimentary breccias are characterized by an increase of Jurassic-Aptian clasts and a decrease of mantle clasts size. Locally, ophicalcite breccias (Fig. 6D) occur that are made up of variably serpentinized, angular lherzolite clasts of various sizes in a calcitic cement (Lagabrielle and Bodinier, 2008). Locally, thin layers of lherzolitic sand accumulate between the clasts. The breccia is poorly stratified and appears to fill large voids opened in the ultramafic basement. Figure 6E shows the most representative facies of the Urdach breccias, polymictic lherzolite-marble breccia. Clasts correspond to various types of high-temperature marble (white, Jurassic; black, Liassic; some are foliated) ranging in size from 1 mm to 10 cm. Lherzolite clasts are generally larger, reaching sizes up to 40 cm. Sorting and bedding are nearly absent. The matrix is mainly a lherzolitic sandstone with numerous small grains of marble. This member also contains meter-scale olistoliths of the same composition as the breccia clasts (Debroas *et al.*, 2010). Thus the Urdach Member corresponds to the sedimentary sequence that records mantle denudation at the end of the rifting stage.

Regional distribution. This member lies north of the Igountze Unit and west of the Urdach mantle outcrop, within the hyperextended domain of the Mauléon Basin (Fig. 3).

Boundaries. The Urdach Member is limited at the base by the lower part of the Flysch de Mixe Formation and on top by the Flysch à Silex Formation (Fig. 3) (Fixari, 1984; Debroas *et al.*, 2010).

Age. The lateral relationship with the Flysch de Mixe Formation suggests a Late Albian to Early Cenomanian age (Tab. 1).

Depositional system. The clast-supported breccias might correspond to the Mutti F3 facies, clast-supported debris flows. The Urdach breccias is characteristic of a to toe-of-slope depositional system (Fixari, 1984; Souquet *et al.*, 1985; Debroas *et al.*, 2010). Due to the predominance of reworked mantle material, these breccias and olistoliths have been interpreted as fault-scarp breccias fed from the east (Debroas *et al.*, 2010), where mantle rocks currently crop out in the vicinity of Urdach (Jammes *et al.*, 2009; Masini *et al.*, 2014; Lagabrielle *et al.*, 2019).

3.4.2 Erretzu Member

Lithostratigraphy and sedimentary description. The Erretzu Member is made up of unorganized conglomerate and breccia (Fig. 6F), imbricated conglomerate with Paleozoic and Upper Triassic pebbles, laminated sandstone with interlayered gravel lags and marls. The beds at the base of the member display erosive geometries, incising the underlying dark marls.

Regional distribution. This member lies north of the Igountze Unit, within the hyperextended domain of the Mauléon Basin (Fig. 3). Its thickness is locally as great as 300 m (Fixari, 1984).

Boundaries. The Erretzu Member rests upon the Lanne Member of the Saint-Palais Formation (Fig. 3). It is overlain by the Flysch à Silex Formation

Age. The stratigraphic position between the Saint-Palais and Flysch à Silex Fms. suggests a Late Albian to Early Cenomanian age for this member (Tab. 1).

Depositional system. The conglomerates have been interpreted as highly concentrated turbidity current deposits, corresponding to conglomeratic proximal channelized flows (Fixari, 1984). Channel overflows are responsible for the development of more distal deposits controlled by tractive mechanisms at the end of the channeled systems (Fixari, 1984). The Erretzu Member corresponds to slope-gullies depositional system (Fixari, 1984). Ten paleocurrents measured in this member indicate a sediment supply towards the WNW (Fixari, 1984).

3.5 Saint-Étienne-de-Baïgorry Formation

Lithostratigraphy and sedimentary description. The Saint-Étienne-de-Baïgorry Formation is laterally equivalent to the Flysch de Mixe Formation. This formation consists of a basal breccia containing polygenetic blocks from 5 cm to 1.5 m in diameter, with an average block size of 50 cm (Fig. 7A). Clasts consist of Upper Triassic igneous rocks and limestone (Muschelkalk facies), Carboniferous limestone, Devonian schist and Upper Albian limestone (Merle, 1974). The Albian limestone contains numerous polyps, orbitolinid foraminifers, algae, and the foraminifer *Hensonia lenticularis.* On the east side of the Saint-Étienne-de-Baïgorry area, in the Honto locality, this formation is composed of pink calcareous breccia with numerous angular to subangular clasts of Paleozoic metasediments (quartzite, schist and micritic limestone) and Upper Albian limestone (clasts between 4 cm and 1 m in diameter; Fig. 7B). More rarely, Upper Triassic igneous rocks clasts are visible. The calcareous to sandy matrix contains flat orbitolinids, polyps and algae (Merle, 1974) suggesting a Late Albian age for this formation.

Regional distribution. This formation is marked by abrupt variations in thickness from zero to 75 m over short distances, and crops out in the Saint-Étienne-de-Baïgorry Unit, at the foot of the Iberian proximal margin.

Boundaries. The Saint-Étienne-de-Baïgorry Formation is delimited by thrusts, separating it from the Aldudes domain to the south and from the Late Triassic deposits of Saint-Jean-Pied-de-Port to the north (Fig. 3).

Age. The fauna suggest a latest Albian to Early Cenomanian age (Merle, 1974; Le Pochat *et al.*, 1978; Tab. 1).

Fig. 7. Field photographs showing (A) clast-supported polygenetic breccia of the Saint-Étienne-de-Baïgorry Formation, composed of igneous rocks and Paleozoic metasediments and minor Upper Albian carbonate platform rocks; (B) matrix-supported polygenetic breccia of the Saint-Étienne-de-Baïgorry Formation made up of Paleozoic clasts and Upper Albian carbonate platform rocks from 2 cm to 1 m in diameter; and (C, D) polygenetic breccias of the Errozaté Formation made up of meter-sized blocks of Upper Albian, Cenomanian and Turonian carbonate platform rocks, Upper Triassic igneous rocks and Paleozoic sedimentary basement. UT: Upper Triassic; P: Paleozoic; Oph: Igneous rocks.

Depositional system. The Saint-Étienne-de-Baïgorry breccias correspond to the Mutti F3 facies, clast-supported debris flows. The scarce occurrence of hyperconcentrate deposits, suggests a rather inefficient transport process. This could result from a hydraulic jump induced by a significant break in the slope. The Saint-Étienne-de-Baïgorry Formation is characteristic of a toe-of-slope depositional system (Saspiturry, 2019). The nature of the clast that are mainly composed of Paleozoic basement shows that these breccias were supplied from the south, *i.e.*, the Paleozoic basement of the Aldudes Massif (Fig. 2B) (Masini *et al.*, 2014).

3.6 Errozaté Formation

Lithostratigraphy and sedimentary description. The Errozaté Formation consists of clast-supported breccia containing clasts derived from the Upper Cretaceous Calcaires des Cañons Formation, Paleozoic metasedimentary basement rocks and Upper Triassic igneous rocks. From base to top, this formation is a succession of pink, red, gray and reddish breccia. The pink breccia is 20 m thick and contains Paleozoic clasts at its base similar to the underlying Mendibelza Formation. The carbonate matrix is rare and slightly sandy. The clasts are angular, smaller than 1 m and consist of Paleozoic metasediments, Late Triassic igneous rocks, uppermost Albian pink limestone with *Hensonia lenticularis* and Melobesioideae and uppermost Albian red detrital limestones with polyps, orbitolinid foraminifers, the foraminifer *Favusella washitensis*, caprinid bivalves and algae (Merle, 1974). The red breccia is 20 m thick and contains large reworked blocks (Fig. 7C) of Upper Albian red limestone with caprinid bivalves and polyps, Lower to Middle Cenomanian dark gray limestone of the Calcaires des Cañons Formation and Late Triassic igneous rocks and rare Paleozoic metasediments (Le Pochat *et al.*, 1978). The overlying gray breccia is 50 m thick and has a carbonate matrix. The clasts consist of Upper Albian red limestone and Upper Cenomanian to Turonian gray limestone of the Calcaires des Cañons Formation, Paleozoic metasediments and Upper Triassic igneous rocks (Fig. 7D) (Merle, 1974). The uppermost reddish breccia is 50 m thick and contains clasts of Coniacian rocks from the Calcaires des Cañons Formation, Paleozoic metasediments and Upper Triassic igneous rocks ranging in size from 1 cm to 3 m.

Regional distribution. This formation crops out south of the Mendibelza and Igountze Units, in the Iberian necking zone (Fig. 3). Its total thickness varies from 50 to 150 m.

Boundaries. This formation unconformably overlaps the Upper Albian third mega-sequence of the Mendibelza Formation (Souquet *et al.*, 1985) and is conformably overlain by the Middle to Upper Coniacian Flysch (Fig. 3; Merle, 1974; Le Pochat *et al.*, 1978).

Age. The stratigraphic correlation of the Errozaté Formation indicates a latest Albian to Late Santonian age (Souquet, 1967; Merle, 1974; Le Pochat *et al.*, 1978).

Depositional system. The slightly sandy carbonate matrix and the matrix-supported texture indicate transportation by debris flows, probably due to partial collapses of a non-stable carbonate platform toward the basin (Durand-Wackenheim *et al.*, 1981). The limy composition of the matrix indicates a calcareous debris flow, probably derived from non-consolidated mud on the platform. This muddy, high-density fluid is responsible for transporting the lithified blocks. The presence of Paleozoic clasts suggests that the debris flows eroded basement rocks from the slope. Thus, the Errozaté Formation is characteristic of a toe-of-slope depositional system (Durand-Wackenheim *et al.*, 1981). The nature of the clast that are mainly composed of Calcaires des Cañons limestones shows that these breccias were supplied from the south, *i.e.*, the domain materialized by the current footwall of the Lakhoura Thrust (Fig. 2B) (Masini *et al.*, 2014).

3.7 Flysch à Silex Formation

Lithostratigraphy and sedimentary description. The Flysch à Silex Formation consists of calcareous turbidites made up of gray marl interbedded with thin beds of sandstone and breccia (Figs. 8A and 8B). The gray silty marls form compact layers ranging in thickness from one to tens of meters (Razin, 1989). In the upper part of the formation, the terrigenous fraction decreases and beds become thinner than 1 m. The coarse fraction is composed of Paleozoic angular clasts (shale, quartz, quartzite and sandstone) and numerous Triassic clasts in the upper part of the formation (red sandstone and argillite, with bipyramidal quartz crystals). The matrix contains reworked benthic microorganisms that increase in abundance upward; these include various foraminifers (orbitolinids, miliolids, textularids, Lituoïdés (Daxia), cuneolines, and rare *Praealveolina* species), echinoderm fragments, molluscs and algae (Razin, 1989). The fine fraction (fine sand and silt) includes peloids, small benthic foraminifers, calcispheres, and spicules. These upper beds have sharp and flat basal surfaces. At the base of the formation, the upper limit of the beds is gradational (Razin, 1989). The base of the Flysch à Silex Formation is intruded by analcime gabbro (teschenite) of Middle Cenomanian age, forming sills several kilometers in extent (Rossy *et al.*, 1992).

Regional distribution. The Flysch à Silex Formation crops out throughout the hyperextended domain (Fig. 3) in thicknesses ranging from 100 m to more than 1000 m (Razin, 1989).

Boundaries. The Flysch à Silex Formation overlies the Upper Albian to Lower Cenomanian Flysch de Mixe Formation following an onlapping relationship (Fig. 3). This basal surface has been identified as the post-rift unconformity throughout the Mauléon Basin (Saspiturry *et al.*, 2019a) and is time equivalent to the post-rift unconformity identified in the adjacent Arzacq Basin (Issautier *et al.*, 2020). On top, this formation is conformably overlains by the Turonian calcareous turbidites of the Flysch Bleu Formation (Fig. 3) (Razin, 1989).

Age. Biostratigraphic markers (Boissonnas *et al.*, 1974; Le Pochat *et al.*, 1976; Richard, 1986; Tab. 1), the stratigraphic position between the older Flysch de Mixe Formation and the overlying Turonian turbidites (Bouquet, 1986; Razin, 1989) and the age of the magmatic sills (Rossy *et al.*, 1992) indicate a Middle to Late Cenomanian age.

Depositional system. The gray marls are deep-basin facies with intercalated calcareous and siliciclastic turbidites. The turbidites display Bouma sequences (Ta-Te) that correspond to low-density turbidity currents. The Flysch à Silex Formation is characteristic of a fine-grained turbiditic depositional system (Razin, 1989; Claude, 1990). Forty measured paleocurrents show that this formation was supplied from the north to northwest (Boissonnas *et al.*, 1974; Le Pochat *et al.*, 1976; Roux, 1983; Razin, 1989; Claude, 1990).

3.8 Bonloc Formation

Lithostratigraphy and sedimentary description. The Bonloc Formation consists of polygenetic clast-supported breccia containing clasts of granulite (70%), garnet gneiss (10%), quartz gneiss (5%), pegmatite (5%), and Devonian and Carboniferous mica schist and quartzite (10%) (Fig. 8C) (Claude, 1990; Jammes *et al.*, 2009; Masini *et al.*, 2014). The lower crustal material reworked in these breccias is derived from the Ursuya granulitic unit (Fig. 8D). Some clasts of Late Triassic reddish sandstone and Albian limestone have been identified (Claude, 1990). Matrix is almost absent and the clasts are very angular (Boissonnas *et al.*, 1974). Clast size ranges from 5 cm to 1.5 m. The unit is interbedded at the base with the Flysch de Mixe Formation and on top with strongly weathered fine- to medium-grained calcareous turbidites comparable to those of the post-rift Flysch à Silex Formation (Saspiturry, 2019).

Regional distribution. The Bonloc Formation lies northeast of the Ursuya granulites, at the transition between the Mauléon Basin Iberian necking zone and hyperextended domain (Fig. 3). It reaches a thickness of nearly 300 m (Claude, 1990).

Boundaries. The Bonloc breccias are displaced southward on the Arberoue Thrust. The top of the formation grades into the upper part of the post-rift Flysch à Silex Formation (Fig. 3).

Age. The Bonloc breccias were previously considered Late Albian to Early Cenomanian due to the presence of uppermost Albian limestone clasts and their lateral relationship with the Flysch à Silex Formation (Boissonnas *et al.*, 1974; Claude, 1990). However, in their upper part, they interfinger with the Flysch à Silex Formation, which implies a Middle to Late Cenomanian age for the uppermost part of this formation (Saspiturry, 2019). When weathered, the Flysch à Silex Formation can be indistinguishable from the Flysch de Mixe Formation, and it was not mapped separately in the Saint-Jean-de-Luz domain before 1980, therefore some authors have considered the Bonloc breccias as part of the Flysch de Mixe Formation (Boissonnas *et al.*, 1974; Claude, 1990).

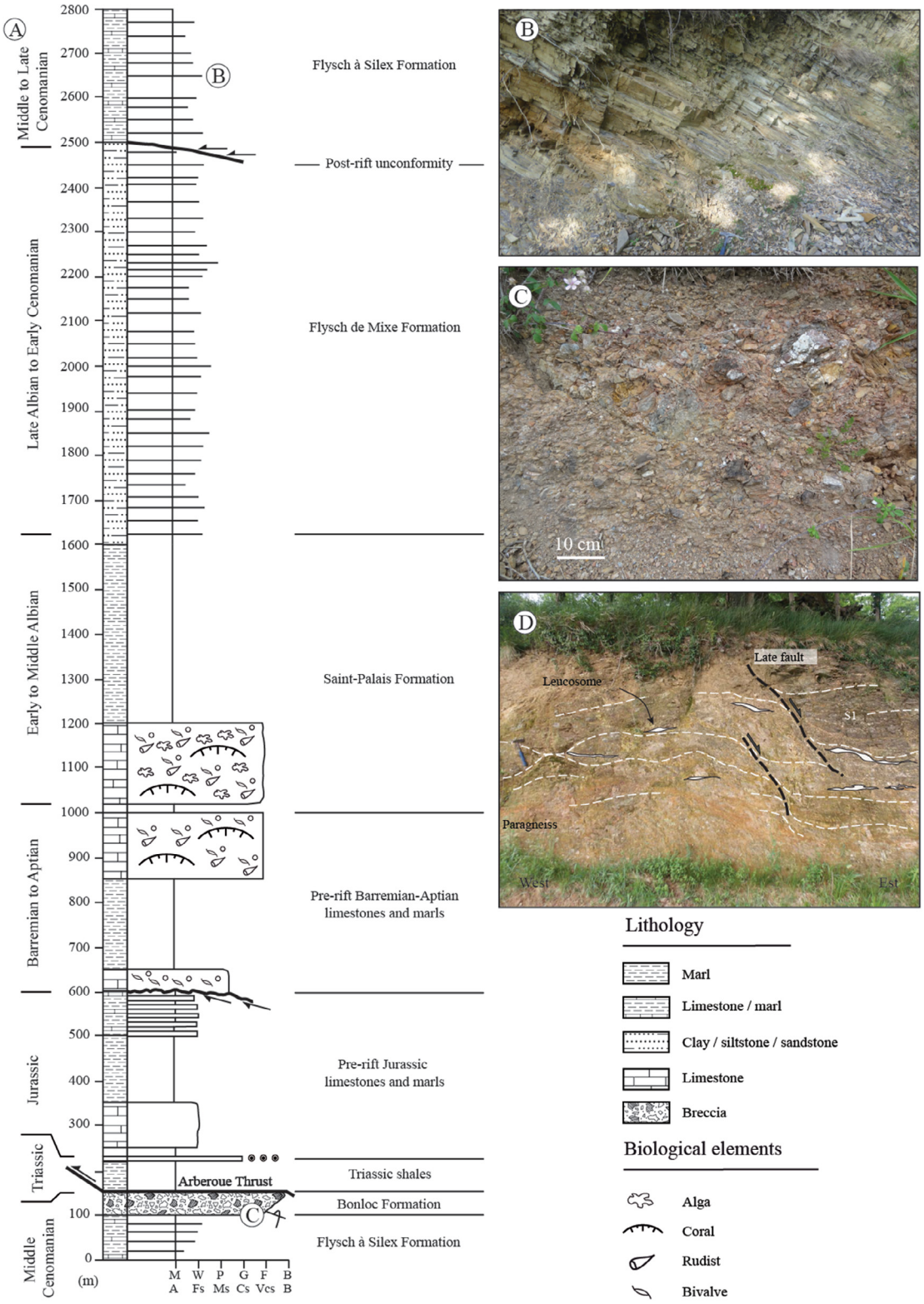

Fig. 8. (A) Schematic lithostratigraphic column of the Arberoue domain (location in Fig. 3); (B) fine-grained calcareous turbidites of the Flysch à Silex Formation displaying incomplete Bouma sequences; (C) polygenetic clast-supported breccia of the Bonloc Formation composed of granulite, gneiss, pegmatite, mica schist and quartzite; (D) exposure of Ursuya granulite with interpretive overlay showing shear zone (broken white lines) and late normal faults (broken black lines).

Depositional system. The clast-supported breccias are indicative of the Mutti F3 facies corresponding to clast-supported debris-flow (Mutti, 1977, 1992). This formation represents a toe-of-slope depositional system (Claude, 1990). The clasts are mainly composed of granulites and gneisses suggesting that these breccias were supplied from the Ursuya granulites (Fig. 2B) (Claude, 1990; Jammes *et al.*, 2009; Masini *et al.*, 2014).

3.9 Hiruraitzeta Formation

Lithostratigraphy and sedimentary description: The Hiruraitzeta Formation can be divided into three units: 65 m of alternating limestone and breccia beds at the base, overlain by a 15-m-thick olistolith and breccia unit and a 15-m-thick breccia unit (Fig. 9A). The lower unit, a mixed detrital-carbonate sequence, consists mainly of alternating breccia with frequent reverse grading and scant matrix and calcareous beds (Fig. 9B). The breccia consists of polygenetic clasts ranging in size from 1 to 8 cm, organized in beds 5 to 15 cm thick, although some breccias form units as thick as 1–2 m with clasts ranging in size from 5 to 30 cm (Fig. 9C). The clasts are angular and include a large range of Upper Triassic igneous rocks, Devonian metasandstone and Carboniferous marble. The first unit is overlain by an olistolith 10–15 m thick consisting of igneous rocks (Fig. 9A), which grades vertically to a 15-m-thick breccia unit (Fig. 9D). The carbonate beds consist of fine-grained facies with wavy laminae grading upward to parallel laminated and massive mudstone.

The upper unit is composed of monogenetic Upper Triassic igneous rocks breccia organized in fining-upward sequences, with bed thickness ranging from 2 to 4 m and the clast size ranging from 2 to 40 cm (Fig. 9D).

Regional distribution. The Hiruraitzeta Formation crops out in the Hiruraitzeta area within the hyperextended domain (Fig. 3). It reaches a thickness of around 100 m.

Boundaries. The base of the Hiruraitzeta Formation overlies the upper part of the Flysch de Mixe Formation, and it grades upward to the upper part of the post-rift Flysch à Silex Formation (Fig. 3; Casteras *et al.*, 1970; Boissonnas *et al.*, 1974; Le Pochat *et al.*, 1976).

Age. Its stratigraphic position between the Flysch de Mixe and Flysch à Silex Fms. indicates that the Hiruraitzeta Formation starts in Late Albian and ends before Late Cenomanian time (Figs. 3 and 9A; Tab. 1).

Depositional system. At the base of the formation, breccias represent hyperconcentrated to gravelly high-density turbidity currents. These facies grade upward to fine-grained calcareous turbidites with planar laminations, then wavy laminations typical of low-density turbidity currents. The presence of olistoliths in the upper part of the formation indicates the proximity of a steep slope producing gravity-flow deposits. The interbedded calcareous turbidites contain typical low-density turbidite facies (Tc to Te) related to their distal position relative to the Aquitaine carbonate platform (to the north). The Hiruraitzeta Formation is characterized by two different depositional systems. The regional source corresponds to a fine-grained turbiditic system (low-density turbidite) interbedded with local toe-of-slope depositional system (high-density turbidity deposits and olistoliths) (Saspiturry, 2019). Ten paleocurrent measurements within the low-density turbidites evidence that they were supplied from the north to north-west as well as the Flysch à Silex turbidites. However, the nature of the clasts within the high-density turbidites and the olistoliths of Upper Triassic material suggests that these latter were supplied from the footwall of the Iholdy transfer fault where the Iholdy diapir develop (Fig. 2A) (Saspiturry, 2019). Thus, this formation is characterized by a bimodal sedimentary source.

3.10 Calcaires des Cañons Formation

Lithostratigraphy and sedimentary description. The Calcaires des Cañons Formation is composed of carbonate and subordinate siliciclastic rocks that are most common in its lower part (Souquet, 1967; Alhamawi, 1992; Ternet *et al.*, 2004). The sedimentary section measured in the Aldudes Unit includes the base of the formation (Saspiturry, 2019; Andrieu *et al.*, 2021), although the lowest part of the Cenomanian deposits, consisting of limonitic limestone microbreccia, is not present there but is described nearby (Le Pochat *et al.*, 1978). In the Aldudes section, a 15 m thick of siliciclastic siltstone to conglomerate rests unconformably on Devonian basement (Fig. 10A). Clasts include Devonian dolomite, quartzite and schist. This unit grades upward to Cenomanian-Turonian carbonate rocks consisting of grainstone with bivalves and peloids alternating with foraminiferal mudstone to packstone containing *Praealveolina* and miliolids (Figs. 10B and 10C) and rudist floatstone (Fig. 10D).

Regional distribution. This formation is present throughout the Iberian proximal margin. Its thickness ranges from 100 to 600 m.

Boundaries. The Calcaires des Cañons Formation rests unconformably on the Paleozoic sedimentary basement of the Aldudes Unit and the Axial Zone as attested by its basal onlap surface (Fig. 3). It is overlain by calcareous flysch of Campanian age (Fig. 3).

Age. The Calcaires des Cañons Formation is assigned to the Cenomanian to Late Santonian based on benthic and planktonic foraminifers and green algae (Souquet, 1967; Merle, 1974; Le Pochat *et al.*, 1978; Alhamawi, 1992; Ternet *et al.*, 2004; Tab. 1). The Cenomanian transgression is marked by the foraminifer association *Praealveolina cretacea*, *Ovalveolina ovum* and *Chysalidina gradata* in the Aldudes section. The basal limonitic limestones are dated from the Early to Middle Cenomanian by the foraminifer association *Trocholina arabica* and *Orbitolina conica* (Merle, 1974; Le Pochat *et al.*, 1978). The overlying siliciclastics are dated from the Middle to Late Cenomanian by the foraminifers *Praealveolina cretacea* and *Ovalveolina ovum.* No biostratigraphic markers date rocks of uppermost Albian to Early Cenomanian age *sensu stricto*, which could be missing. However, the toe-of-slope Saint-Étienne-de-Baïgorry breccias and the lowermost part of the Errozaté breccias, which are both supplied from the Calcaires des Cañons platform, are characterized by the presence of uppermost Albian to Lower Cenomanian limestones clasts. Thus, the Calcaires des Cañons carbonate platform started to developed since the uppermost Albian as along the whole Pyrenean Axial Zone (Andrieu *et al.*, 2021). Two hypotheses can be put forward to explain the

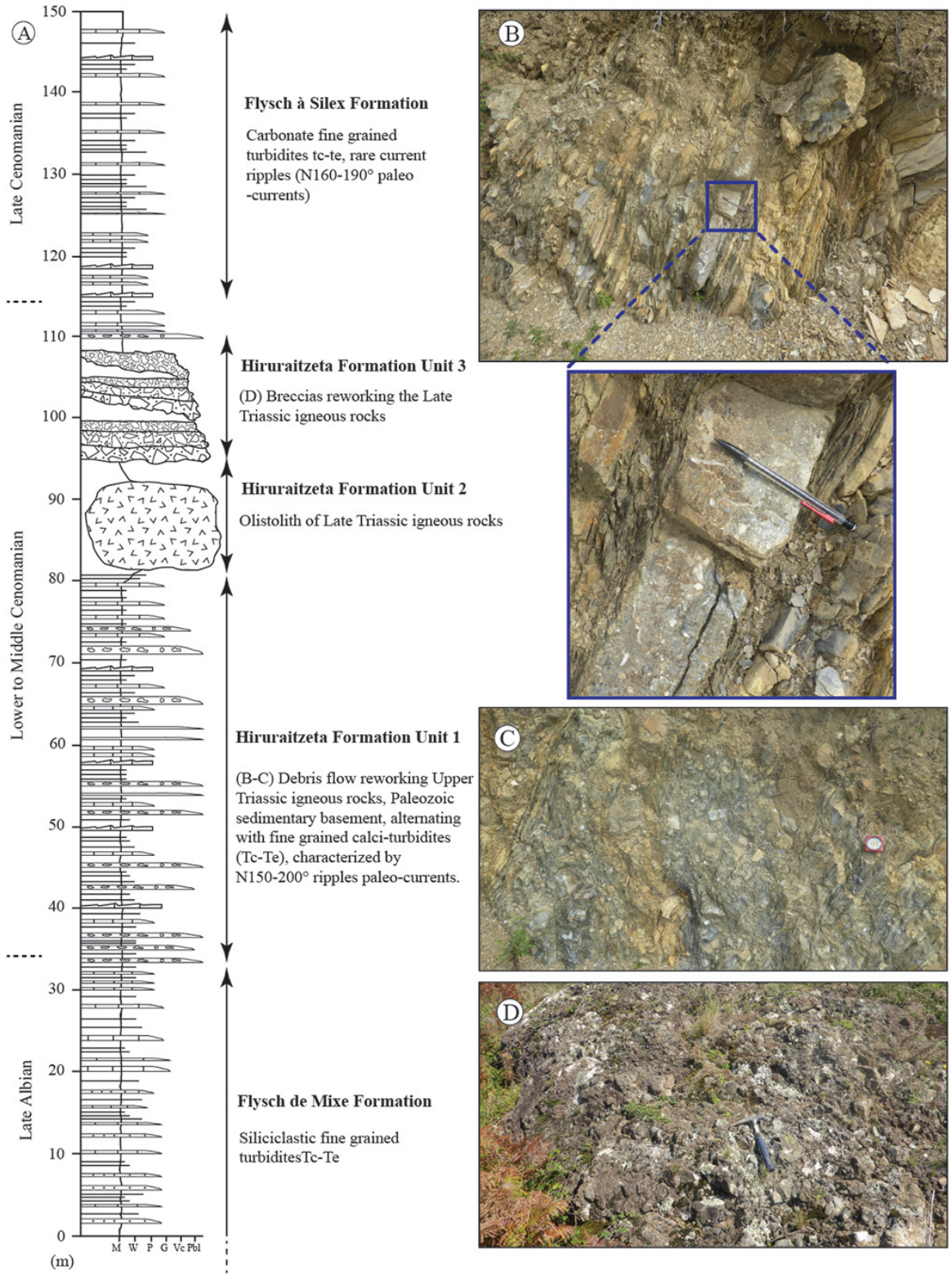

Fig. 9. Stratigraphy and lithology of the Hiruraitzeta Formation (A) Lithostratigraphic column at Hiruraitzeta (location in Fig. 3); (B) fine-grained calcareous turbidites with incomplete Bouma sequences, interfingering with out-of-sequence clast-supported polygenetic breccia with clasts of Paleozoic metasediments and Late Triassic igneous rocks; (C) meter-thick polygenetic breccia with clasts of Paleozoic metasediments and Late Triassic igneous rocks; (D) monogenetic clast-supported breccia of Late Triassic igneous rocks.

fact that the uppermost Albian Calcaires des Cañons transgressive prism does not crop in the Western Pyrenees: (1) this sedimentary succession has been completely eroded and reworked in the toe-of-slope breccias, localized in the Lakhoura detachment hanging-wall, leaving a hiatus of latest Albian to Early Cenomanian age or (2) the uppermost Albian transgressive prism is buried in the footwall of the Lakhoura Thrust.

Depositional system. The basal siliciclastic unit is a transgressive sequence marked in its lowermost part by an erosive conglomerate that reworks the underlying substratum. Based on the limestone texture and faunal assemblages, the carbonate platform facies is interpreted as deposited in inner ramp-lagoon to shoreface depositional system (Souquet, 1967; Merle, 1974; Alhamawi, 1992; Andrieu *et al.*, 2021).

4 Paleogeographic reconstructions and considerations in lower crust and mantle exhumation assessments

4.1 Evolution of the sedimentary environment during hyperextension and post-rift cooling

4.1.1 Albian syn-rift stage

During Early Albian time, the Mauléon Basin was affected by the onset of continental crust thinning and tectonic subsidence (Figs. 11A and 12A) (Jammes *et al.*, 2009; Masini *et al.*, 2014; Tugend *et al.*, 2015; Lescoutre *et al.*, 2019, 2021; Gómez-Romeu *et al.*, 2019; Lescoutre and Manatschal, 2020). This first syn-rift deformation stage affected the northern edge of the Mauléon Basin through the development of the south-dipping Saint-Palais detachment (Saspiturry *et al.*, 2019a). As previously discussed, this extensional detachment offsets the southern basin floor and induces a regional northward tilt of the whole Iberian margin (Fig. 11A). This tilting led to the northward *décollement* of the entire pre-rift sedimentary cover upon the Keuper layer and the subsequent development of a very asymmetric basin floor (Saspiturry *et al.*, 2019a, 2021). This gravity-driven tectonic denudation was a major stage of the Pyrenean rifting stage that exposed the Paleozoic basement of the Iberian proximal margin and necking zone (Lagabrielle *et al.*, 2010; Saspiturry, 2019). Today the displaced pre-rift cover crops out in the inverted Croissant d'Arberoue, Arbailles and Chaînons Béarnais Units (Fig. 2B), but it is mostly buried under the Cretaceous syn-rift to post-rift cover within the hyperextended domain (Corre *et al.*, 2016; Teixell *et al.*, 2016; Saspiturry *et al.*, 2019a).

The onset of the pre-rift cover displacement seems to be synchronous with local diapirism along the Iberian margin of the Mauléon Basin (Canérot, 1988, 1989; Canérot and Lenoble, 1993; James and Canérot, 1999; Canérot *et al.*, 2005). Similarly, the eastern Mauléon Basin contains an Upper Albian system of salt anticlines (salt walls) separated by synformal mini-basins (Chaînons Béarnais) beneath a discontinuous Jurassic-Cretaceous pre-rift cover displaced by gliding into the hyperextended domain (Labaume and Teixell, 2020).

Immediately after the gravitational sliding of the pre-rift cover, the Albian Mendibelza Formation began to accumulate, incorporating clastic material from the freshly denudated Iberian basement. During Albian time, the Mendibelza coarse-grained turbiditic depositional system (Boirie, 1981; Fixari, 1984; Souquet *et al.*, 1985) accumulated on the Iberian necking zone, as evidenced by the ~2000 m thick conglomerates. The source area of these coarse-grained deposits was close to the source-canyon, suggesting a narrow siliciclastic platform/basin transition, typical of active tectonics. Indeed, these deposits mark the initial syn-rift succession of the Mauléon Basin. They are scattered along a steep slope at the transition between the Iberian proximal margin and the Iberian necking zone. Paleocurrent measurements from the Mendibelza Formation show that the conglomerates were fed by a sedimentary source to the southwest (Boirie, 1981; Fixari, 1984). The composition, size and roundness of the clasts suggest a relatively short sediment transport on the margin through a fan-delta depositional system reworking Paleozoic metasedimentary units in an uplifted and emergent area to the south in the present-day Axial Zone (Early Cretaceous Iberian proximal margin) (Figs. 11A and 12A). None of that source region is preserved as it has been overprinted by the Pyrenean shortening (Saspiturry *et al.*, 2019b). Towards the north, the Mendibelza coarse-grained turbiditic depositional system was adjacent to the coeval Saint-Palais deep-basin depositional system composed of diluted turbidites and decantation marls (Figs. 11A and 12A). This abrupt change between these two different depositional systems, characterized by the near-absence of high-density turbidites, evidences the very poor transportation efficiency of the Iberian margin sedimentary system during the whole Albian. To the north, in the hyperextended domain, the Iholdy N20°-trending transfer zone (Canérot, 2008, 2017), inherited from the Permian post-orogenic extension (Saspiturry *et al.*, 2019b), bounds an uplifted area and a depocenter with sedimentation of deep-basin marls during the Albian (Fig. 11A). The Albian Mendibelza and Saint-Palais formations are also characterized by a significant northward thickness increase with thicknesses ranging from 1 km at the foot of the Iberian margin to 4 km at the foot of the Saint-Palais Thrust in the hyperextended domain (Figs. 11A and 12A). This pattern results of the development of a significant depocenter in the hanging-wall of the Albian Saint-Palais detachment (Fig. 12A). The eastern Mauléon Basin hyperextended domain locally hosted the deposition of the Lanne Member slope-gullies depositional system. These deposits, fed from the southeast, traveled onto the decantation marls of the hyperextended domain (Fig. 11A).

In the western part of the Mauléon Basin, the pre-rift sedimentary deposits were dismembered during the earliest Albian gliding displacement, forming a submarine scarp of pre-rift cover between the Iberian margin necking zone and the hyperextended domain. Throughout the Albian, erosion of this scarp (deep-marine bypass or no-deposition area in Fig. 11A) led to the deposition of debris flows and sedimentary klippen of the Bustince Formation. This toe-of-slope depositional system represents the only deposits that reworked the pre-rift cover within the syn-rift sedimentary pile of the Mauléon Basin. Other than this instance, the Mauléon pre-rift cover seems to have glided into the basin core without being significantly fragmented (Lagabrielle *et al.*, 2010, 2020; Corre *et al.*, 2016; Asti *et al.*, 2019; Saspiturry *et al.*, 2021).

On the conjugate European margin, the Saint-Palais shallow carbonate platform developed throughout the Albian grading distally into the Saint-Palais deep-basin marls (Figs. 11A and 12A) (*e.g.*, Saspiturry *et al.*, 2019a and

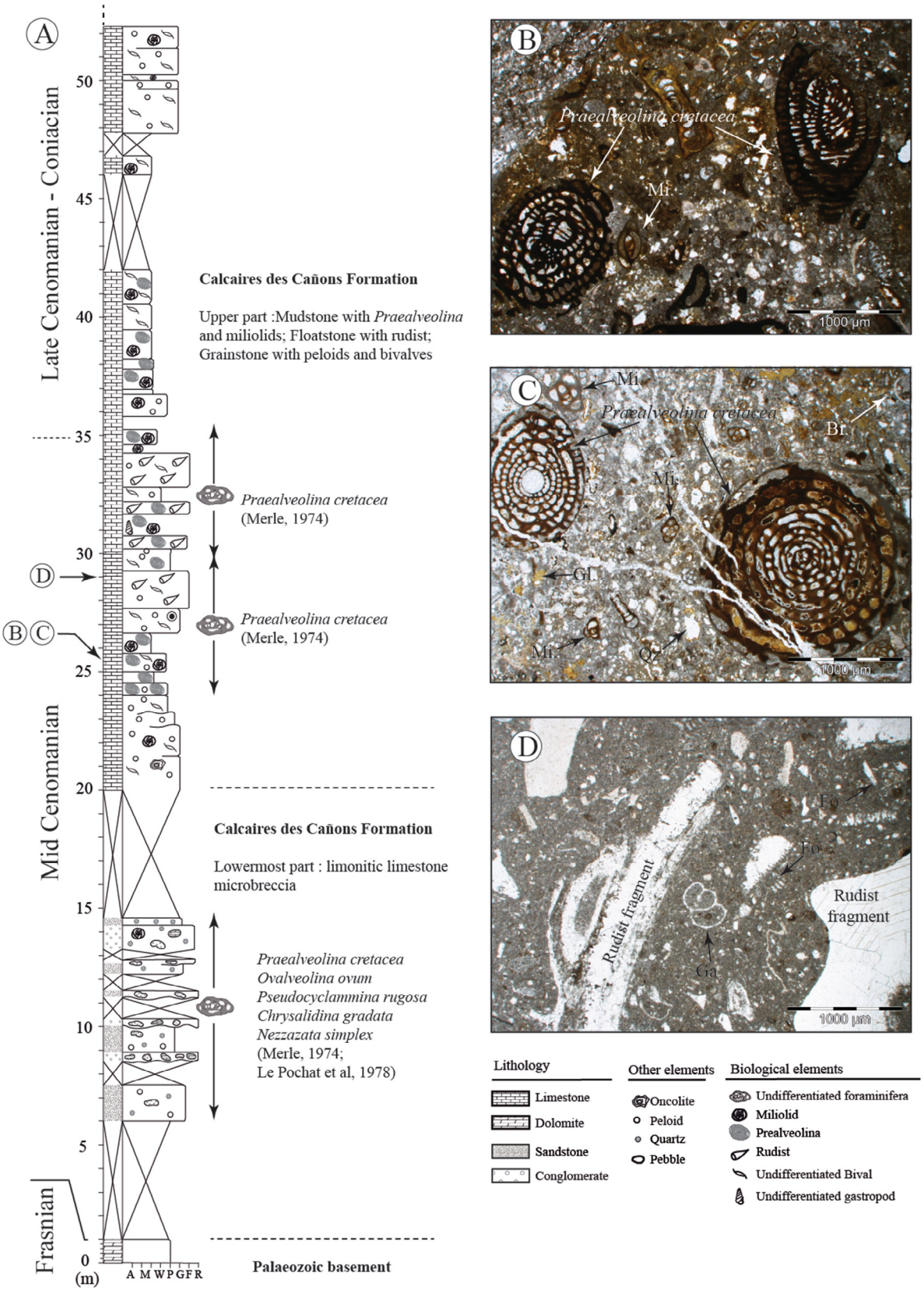

Fig 10. (A) Sedimentary log of the Calcaires des Cañons carbonate platform; (B, C) wackestone to packstone with *Alveolina*, miliolids (Mi.), bivalves (Bi.), quartz (Qz), and glauconite (Gl.); (D) wackestone rich in rudist fragments with well-preserved gastropods (Ga.) and foraminifers (Fo.) (from Saspiturry, 2019; Andrieu *et al.*, 2021).

references therein). From Early to Late Albian time, the depositional systems recognized from both sides of the Mauléon Basin shed light on its asymmetrical morphology driven by the development of the Saint-Palais detachment. Indeed, the Mauléon southern necking zone records the deposition of coarse-grained detrital sedimentation and was mainly supplied with sediment from the Iberian proximal margin (Figs. 11A and 12A). On the other side, the hyperextended domain records sedimentation of deep-basin marls of the Saint-Palais Fm. derived from the carbonate platforms located on the European margin.

4.1.2 Latest Albian to Early Cenomanian mantle denudation stage

The Mauléon Basin was affected by significant paleogeographic and tectonic reorganization starting in the latest Albian, as indicated by the development of two north-dipping detachments (Saspiturry *et al.*, 2019a) and the westward widening of the basin (Razin, 1989; Claude, 1990) (Fig. 11B). We will see later that after this major reorganization, the detrital formations are then fed from the emerged footwalls of the detachments, while the hanging-wall to the north remains submerged (European margin).

The pair of newly formed detachments were defined by Jammes *et al.* (2009) and Masini *et al.* (2014) as the South Mauléon Detachment (SMD) and the North Mauléon Detachment (NMD). These extensional structures were responsible for defining the Saint-Étienne-de-Baïgorry, Mendibelza, Arbailles and Igountze structural units in the Iberian margin necking zone (Fig. 2). The latest Albian to Early Cenomanian age of these detachments is attested by the absence of wedge-shaped syn-tectonic growth strata in the 2000-m-thick Lower to Middle Albian syn-rift sequence of the Mendibelza Formation (Saspiturry *et al.*, 2019a) and the 98 Ma cooling age obtained on the SMD by Hart *et al.* (2017).

At this time, the southern Mauléon Basin received numerous debris-flow deposits derived from the footwalls of these north-dipping detachments (Masini *et al.*, 2014). These toe-of-slope depositional systems are represented by the Bonloc, Saint-Étienne-de-Baïgorry and Errozaté Fms. as well as the Erretzu Member (Fig. 11B). The presence of Paleozoic and uppermost Albian Calcaires des Cañons limestone clasts suggests that these debris flows are supplied both by the carbonate platform localized in the SMD footwall as well as basement rocks from the slope. The development of the SMD and NMD detachments was responsible for a spectacular basin floor inversion that changed the tilt of the Iberian basement from northward to southward. This structural change generated a basin structural high that persisted until the Santonian (Saspiturry *et al.*, 2019a), as attested by the nondeposition of syn-rift to post-rift sediments over the Arbailles/Chaînons Béarnais Massifs (Fig. 11B). From the latest Albian to the Early Cenomanian, the sedimentary sources also dramatically changed. Sedimentary flux from the Iberian proximal margin was restricted to debris flows reworking carbonate rocks from the Iberian margin platform (Figs. 11B and 12B). The hyperextended domain, previously fed by a fan delta on the Iberian margin, became supplied from a western source. The uppermost Albian westward widening of the basin induced the development of a deltaic depositional system to the west of the Mauléon Basin, which was previously emergent (Razin, 1989), that was responsible for the deposition of the Flysch de Mixe fine-grained depositional system (Figs. 11B and 12B). This new sedimentary flux deposited up to 2000 m of low-density turbidites and deep-basin marls in the hyperextended domain (Figs. 11B and 12B). At that time, the Iholdy, Saison and Barlanès transfer zones partitioned this sedimentation into two main turbiditic depocenters delimited by diapiric structures responsible for differential subsidence (Fig. 11B). Indeed, these transfer zones also localized diapirism such as the Iholdy and Roquiague diapirs (Canérot, 2008). Thus, the debris flows and olistoliths of Triassic material within the Hiruraitzeta Formation, were probably derived from either the NMD detachment footwall or the Iholdy diapir that uplifted Triassic evaporites and igneous rocks to the seafloor (Fig. 11B).

This stage also saw the advent of deep crustal and subcontinental mantle material in the mantle denudation sedimentary sequence. The Ursuya granulite to the west and the Urdach subcontinental mantle to the east reached the seafloor by denudation on the NMD (Fig. 11B). The debris flows of the Bonloc Formation toe-of-slope depositional system, containing reworked clasts from the Ursuya granulite, correspond to breccias derived from the western part of the NMD footwall. These breccias grade northward to low-density turbidites of the Flysch de Mixe fine-grained turbiditic depositional system (Fig. 11B). On the other side of the basin, the debris flows and olistoliths, of the Urdach Member toe-of-slope depositional system, reworked clasts derived from the Urdach mantle body (Figs. 11B and 14B). These observations show that mantle denudation occurred within the Mauléon Basin during the latest Albian and Early Cenomanian.

On the European margin, the shallow carbonate platform shifted significantly northward, resulting in N-S widening of the turbiditic basin (Figs. 11B and 12B) (*e.g.*, Saspiturry *et al.*, 2019a and references therein). This carbonate platform graded southward to the Flysch de Mixe fine-grained turbiditic depositional system within the hyperextended domain.

4.1.3 Middle to Late Cenomanian post-rift stage

From Middle Cenomanian to Santonian time, the Mauléon Basin underwent post-rift subsidence and a carbonate platform developed on both margins (Fig. 12C). The SMD and NMD become inactive, accommodating no more crustal thinning (Figs. 11C and 12C) (Jammes *et al.*, 2009; Masini *et al.*, 2014). Along the Iberian margin, the Calcaires des Cañons platform continued to provide massive amounts of clastic material to debris flows of the toe-of-slope Errozaté Formation (Figs. 11C and 12C). Since the basin was not filled completely at the end of hyperextension, the NMD fault scarp continued to contribute to the hyperextended domain sedimentary flux, though at a lower rate. Resedimented clasts in the upper part of the post-rift Bonloc and Hiruraitzeta Fms., exposed in the inactive NMD hanging-wall, are present in the Flysch à Silex fine-grained turbiditic depositional system. Whereas the hyperextended domain was previously supplied from the west during the syn-rift stage, the post-rift calcareous turbidites of the Flysch à Silex Formation were supplied from the north and derived from the Calcaires des Cañons carbonate platform on the European margin (Figs. 11C and 12C) (Razin, 1989; Saspiturry *et al.*, 2019a).

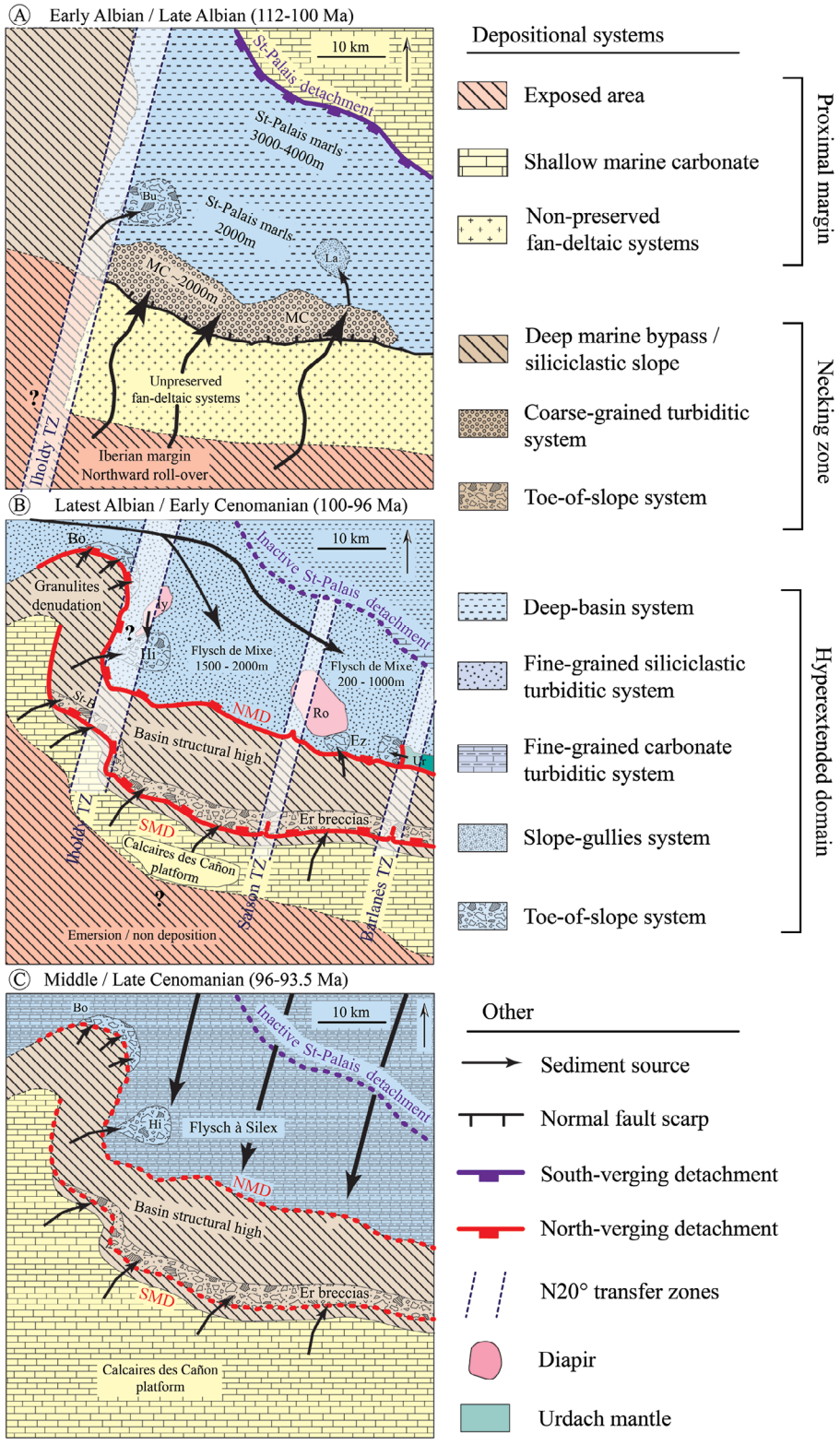

Fig. 11. Palinspastic restorations of the Mauléon hyperextended rift basin showing the main depositional systems, active faults and sedimentary fluxes from the Albian to the Late Cenomanian. (A) Early to Late Albian; (B) latest Albian to Early Cenomanian; (C) Middle to Late Cenomanian. Bu: Bustince Formation; MC: Mendibelza Formation; La: Lanne Member; SMD: South Mauléon Detachment; NMD: North Mauléon Detachment; Er: Errozaté Formation; St-B: Saint-Étienne-de-Baïgorry Formation; Bo: Bonloc Formation; Hi: Hiruraitzeta Formation; Ez: Erretzu Member; Ur: Urdach Member; Iy: Iholdy diapir; Ro: Roquiague diapir.

4.2 Implications for continental crust thinning and mantle exhumation during the Early Cretaceous

4.2.1 How the palaeogeographic reconstructions bring new constrains on the mode of basin opening: pull-apart vs. orthogonal rifting?

The understanding of thinning of the western Pyrenean continental crust during Early Cretaceous has drastically evolved during the last decades. The Mauléon Basin was formerly regarded as a pull-apart basin where continental crust thinning was mainly accommodated by sinistral strike-slip deformation resulting in the formation of syn-rift normal faults oriented N120° and N20° (Canérot and Delavaux, 1986; Canérot, 1988, 2008, 2017; Debroas *et al.*, 2010). Recent work has shown that crustal thinning was mainly controlled by orthogonal rifting processes, which gave rise to detachment systems oriented N120° that were responsible for hyperextension of the continental crust and mantle denudation (Lagabrielle and Bodinier, 2008; Jammes *et al.*, 2009; Masini *et al.*, 2014; Tugend *et al.*, 2015; Lescoutre *et al.*, 2019, 2021; Saspiturry *et al.*, 2021).

The pull-apart model (*e.g.*, Canérot, 2017) seems to be not supported by the palaeogeographic reconstructions since both the N120° (Saint-Palais Fault, NMD, SMD) and N20° (Iholdy, Saison and Barlanès) syn-rift structures should be active at the same time to form conjugated strike-slip faults. Moreover, the sedimentary infill of the Mauléon Basin should be derived from all the pull-apart margins at the same time, but this is not supported by the paleogeographic reconstructions. The paleogeographic reconstructions presented in this work seem to argue in favor of hyperextension models rather than the pull-apart one. Indeed, the sedimentary infill of the Mauléon Basin share significant similarities with current and fossil hyper-extended passive margins that record the deposition of shallow marine systems on the proximal margin (Alves *et al.*, 2002, 2009) while the hyperextended domain record the deposition of toe-of-slope deposits reworking the footwall of the detachments responsible for sub-continental mantle denudation (Masini *et al.*, 2011, 2012; Alves and Cunha, 2018; Ribes *et al.*, 2019). Moreover, the domain composed of shallow marine depositional system to the north of the Saint-Palais structure is replaced by a fine-grained turbiditic depositional system during the latest Albian. This northward widening of the sedimentation area, highlighted by the paleogeographic reconstructions, is not consistent with a pull-apart system that should be characterized by a W-E widening. This observation supports the models of orthogonal rifting and seems to be the result of the successive activation of the SMD and NMD detachments.

The Mauléon Basin share similarities with the adjacent Basque-Cantabrian Basin that suffered hyperextension of the continental crust and mantle exhumation during the Albian to Cenomanian (DeFelipe *et al.*, 2017; Pedrera *et al.*, 2017, 2020; Garcia-Senz *et al.*, 2019). Indeed, the Basque-Cantabrian Basin, is also characterized by a southward widening of the sedimentation area during the Late Albian as evidenced by: (1) the southward retrogradation of the Ramales carbonates and Valmaseda deltaic system above more fluvial units and (2) the southward expansion of fluvial, transitional to shallow marine Utrillas and Escucha Formations above more continental units and basement rocks (Martín-Chivelet *et al.*, 2002; Poprawski, 2012). As in the Mauléon Basin, this N-S widening is time equivalent to the activation of a detachment system responsible for mantle denudation (Pedrera *et al.*, 2017, 2020; Garcia-Senz *et al.*, 2019).

4.2.2 Bimodal exhumation of the ursuya granulite

The paleogeographic reconstructions proposed in this review (Fig. 11) indicate that the Ursuya granulite reached the seafloor in the transitional area between the Saint-Jean-de-Luz deltaic systems in the proximal margin and the proximal turbiditic basin (Fig. 12B). Thus, the exhumation of the granulite did not occur in the most distal part of the basin, but in a domain that had not undergone hyperextension of the continental crust (necking zone). This circumstance differs from classical magma-poor passive margins (*e.g.*, Tugend *et al.*, 2018; Péron-Pinvidic *et al.*, 2019). The question then arises why the Ursuya granulite was denudated in this peculiar paleogeographic position.

A pre-Triassic age for the ductile deformation within the granulites and migmatites from the Ursuya Massif was confirmed by Ar/Ar ages on biotite indicating that these rocks cooled below the biotite Ar closure temperature of ~300° at 200 Ma (Masini *et al.*, 2014). Available U-Pb ages indicate that high-temperature metamorphism occurred between 295 and 274 Ma (Hart *et al.*, 2016; Vacherat *et al.*, 2017; Lemirre, 2018; Vielzeuf *et al.*, 2021). During this period, strain was localized within the extensional Louhossoa shear zone (Figs. 13A and 14A), allowing the exhumation of granulite from ca. 18 km depth to the upper crust (Lemirre, 2018; Saspiturry *et al.*, 2019b). Pressure-temperature estimates from other north Pyrenean Massifs support this interpretation (de Saint Blanquat *et al.*, 1990; de Saint Blanquat, 1993; Delaperrière *et al.*, 1994; Cochelin *et al.*, 2017; Lemirre, 2018). Saspiturry *et al.* (2019b) suggest that the top of the Ursuya dome lay under 5–6 km of sediments at the end of the Triassic. The paleo-geotherm was probably higher than 30°C/km, and more likely around 50–60°C/km at the end of the Triassic (Saspiturry *et al.*, 2019b), as it corresponds to a significant rifting and magmatic event at the scale of the Western Europe (Leleu *et al.*, 2016). This paleo-geotherm and the inferred presence of 5 km of sedimentary cover at the end of the Triassic are consistent with the paleothermometric study by Masini *et al.* (2014), which highlighted a closure of the biotites Ar-Ar system at 200 Ma.

Following the Permian post-orogenic extension and the Triassic thermal event recorded within the Pyrenees, the Ursuya granulite was buried under 500 to 1000 m of Jurassic to Aptian limestone and marl. Thus, at the onset of the Early Cretaceous rifting, the Ursuya granulite was buried under 6–7 km of sediments. The displacement by gliding of the pre-rift cover along the Upper Triassic salt *décollement* that occurred on the Iberian margin at the beginning of the Albian rifting (Bouquet, 1986; Lagabrielle *et al.*, 2010, 2020; Teixell *et al.*, 2016; Saspiturry *et al.*, 2019a, 2021; Labaume and Teixell, 2020) subtracted the Upper Triassic to Aptian cover from the Ursuya granulite. The final exhumation and denudation of the granulite was achieved during the latest Albian to Early Cenomanian along the NMD, which reactivated the shear zone on the northern and western edges of the Ursuya dome defined by Saspiturry *et al.* (2019b) (Figs. 13B and 14B). Reactivation of this shear zone during the hyperextension stage finally brought the granulite to the seafloor at the end of the Early

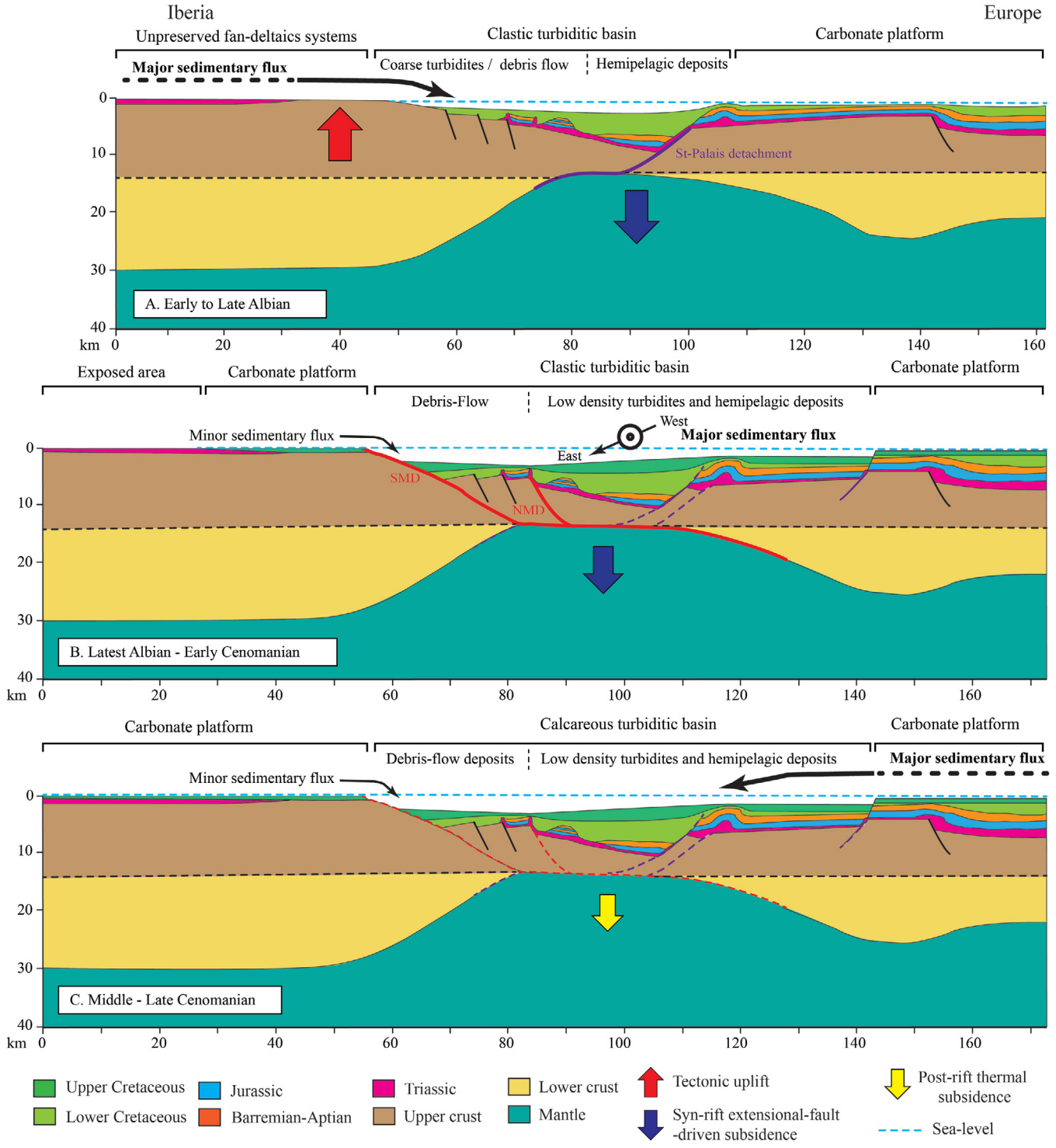

Fig. 12. Palinspastic restorations of the crustal-scale balanced cross-section of Saspiturry *et al.* (2020a) shown in Figure 2D, highlighting the main sedimentary fluxes. (A) Early to Late Albian; (B) latest Albian to Early Cenomanian; (C) Middle to Late Cenomanian.

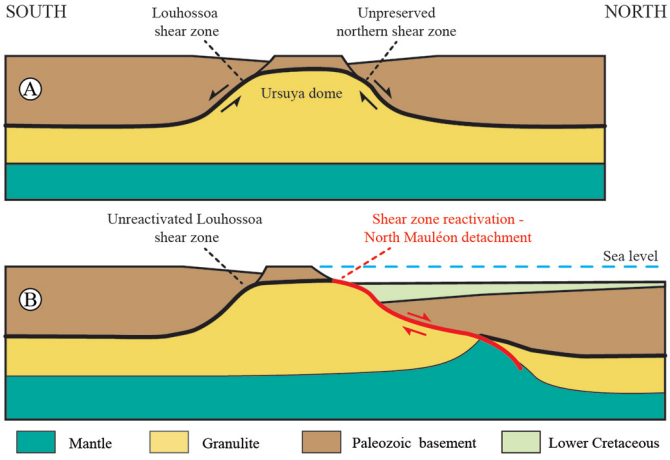

Fig. 13. Schematic restoration of a N-S cross-section through the Ursuya granulitic dome (A) at the end of Permian post-orogenic extension and (B) at the end of Cretaceous hyperextension. Not to scale.

Cretaceous. The Bonloc toe-of-slope-breccias registered the exhumation of the Ursuya granulite by gravity-flow deposits derived from the footwall of the NMD (Masini *et al.*, 2014). Thus, exhumation of the Ursuya granulite took place in two stages: a Permian post-orogenic exhumation within a metamorphic dome and an Early Cretaceous exhumation and denudation during continental rifting. In this interpretation, the Louhossoa shear zone was active during the Permian post-orogenic extension and was not reactivated during Early Cretaceous hyperextension. Thus, the presence of this inherited Permian domal structure led the Ursuya granulite to be exhumed in an unusual position regarding classical basins affected by hyperextension of the continental crust, as evidenced by our paleogeographic reconstructions.

4.2.3 Along-strike discrepancy between crustal thinning and mantle denudation

Although the paleogeographic reconstructions presented in this work clearly support that orthogonal rifting occurred during the Albian to Early Cenomanian, the Mauléon Basin displayed a significant E-W variable amount of stretching at the end of the hyperextension stage (Fig. 14). Our paleogeographic reconstructions show that the amount of crustal thinning increased from west to east. Indeed, the westernmost part of the Mauléon Basin was emergent during the Albian (Fig. 11A) and then became a shallow marine deltaic system from the latest Albian to Early Cenomanian (Fig. 11B). These results are consistent with the balanced cross-section of Lescoutre and Manatschal (2020) evidencing that the continental crust was unusually thick (~20–30 km) at the end of rifting in this domain.

Towards the east, in between the Iholdy and Saison transfer zones (Fig. 2C), our reconstructions demonstrate that this domain was affected by a more important amount of continental crust stretching than the westernmost part of the basin. Indeed, this domain corresponds to the main syn-rift depocenter where deep-basin marls accumulated during the Albian (Fig. 11A) followed by low-density turbidites during the latest Albian to Early Cenomanian (Fig. 11B). Although continental crust thinning was intense in this part of the basin, as evidenced by the positive Bouguer gravity anomaly, reworked clasts of mantle rock were absent from the syn-rift succession. So, mantle denudation might not have happened between the Iholdy and Saison transfer zones. This hypothesis is consistent with the balanced cross-sections east of the Ursuya granulite indicating that hyperextension of the continental crust occurred but that mantle was not denudated (Saspiturry *et al.*, 2020a).

Further east, in the vicinity of the N20° Barlanès Transfer Zone, the paleogeographic reconstructions clearly demonstrate that mantle denudation occurred (Fig. 11B). Indeed, clasts of subcontinental mantle rocks have been reworked into the uppermost Albian to Lower Cenomanian Urdach breccias (Fig. 11B). This observation is also supported by the balanced cross-sections available on the Chaînons Béarnais indicating that mantle denudation occurs (Teixell *et al.*, 2016; Gómez-Romeu *et al.*, 2019; Lescoutre and Manatschal, 2020).

In this volume, Lescoutre and Manatschal (2020) offer an explanation for the variation in crustal thinning across the Mauléon Basin. They suggest that the variation was linked to the overlapping of two Early Cretaceous Rift segments corresponding respectively to the V-shaped, westward-opening Basque-Cantabrian and eastward-opening Mauléon Basins. There, continental crust thinning was partitioned into the nearest basin leaving the crust between them relatively undeformed. Although Lescoutre and Manatschal (2020) bring significant new constraints to the problem of discrepant crustal thinning in the Western Pyrenees, the question remains as to why and how the mantle was denudated at the end of hyperextension only in the Urdach area.

Workers agree on the fact that mantle denudation occurred locally in the easternmost part of the Mauléon Basin, but disagree on the genesis of the Urdach breccias. These have been interpreted as being derived from the footwall of (1) a N20° submarine scarp corresponding to the Barlanès transfer zone (Debroas *et al.*, 2010), (2) a north-dipping detachment oriented approximately N120° (Jammes *et al.*, 2009; Masini *et al.*, 2014) or (3) a domal tectonic contact between mantle and crust that could dip either west or north (Lagabrielle *et al.*, 2019). As the breccias are derived from the dismantling of the Urdach mantle to the east, we infer a west-dipping submarine paleoscarpment during the latest Albian and Early Cenomanian (Fig. 11B). Such a geometry has been imaged on the present-day magma-poor Angola and Brazil passive margins (Péron-Pinvidic *et al.*, 2015). Indeed, Péron-Pinvidic *et al.* (2015) showed that mantle denudation can occur along relay zones oblique to the main direction of extension. In these peculiar domains, generally localized along inherited lineaments, the main detachment systems branch into the transverse relay zones and lead to mantle exhumation oriented oblique to the main rift direction. Thus the N20° Barlanès transfer zone, an inherited Permian Normal Fault (Fig. 14A) like those along the Bidarray Rift system (Saspiturry *et al.*, 2019a), may have been reactivated during hyperextension. This reactivated fault could have acted as a relay zone branching off the NMD, allowing mantle exhumation oblique to the Mauléon Rift axis (Fig. 14B). This interpretation could reconcile the previously proposed models.

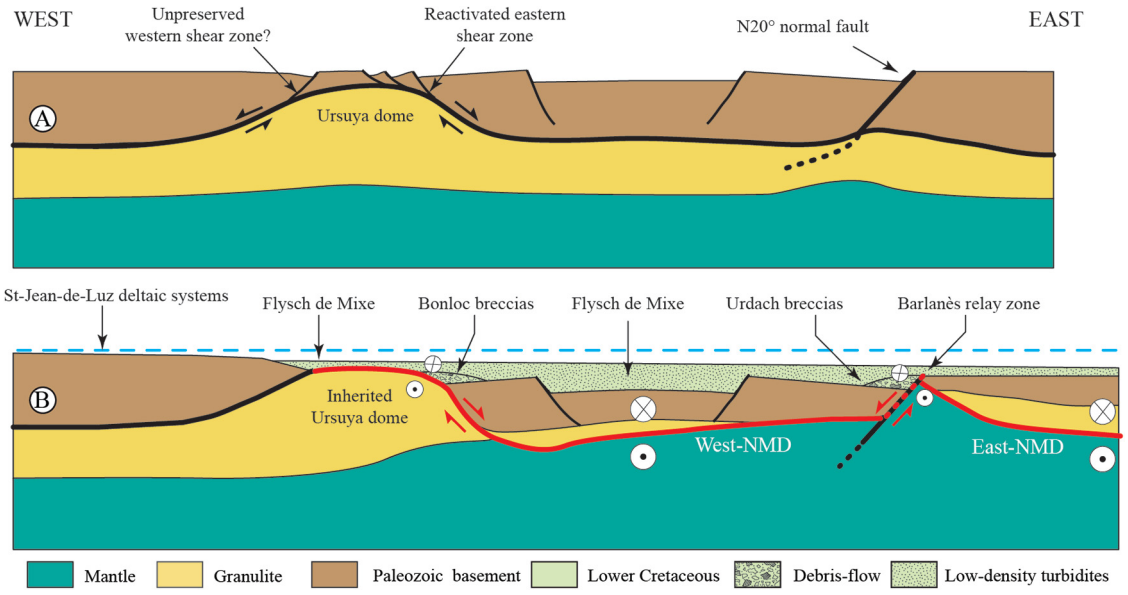

Fig. 14. Schematic restoration of a W-E cross-section through the Ursuya granulitic dome and the Mauléon Basin hyperextended domain (A) at the end of Permian post-orogenic extension and (B) at the end of Cretaceous hyperextension. Not to scale.

5 Conclusion

The Mauléon Basin records hyperextension of the continental crust during the Albian that led to mantle denudation during the latest Albian to Early Cenomanian. The paleogeographic maps proposed here unravel the evolution of sedimentary sources and depositional systems during hyperextension. From Early to Late Albian time, the basin was primarily supplied from the Iberian proximal margin, which was tilted north as the result of the south-dipping Saint-Palais detachment. The steep slope of this margin led to the deposition of nearly 2000 m of conglomerate at the foot of the Iberian necking zone, which transitioned abruptly into low-density turbidites and deep-basin marls accumulating in the hyperextended domain. From the latest Albian to Early Cenomanian, the development of north-dipping detachment systems affecting the Iberian margin was responsible for the local denudation of the subcontinental mantle, which contributed clasts into the Urdach breccias. During this period, minor footwall-derived debris-flow deposits developed at the foot of the SMD in the Iberian necking zone and the NMD in the hyperextended domain. However, the majority of the sedimentary flux into the hyperextended domain was supplied from the west by deltaic systems that produced the siliciclastic low-density turbidites of the Flysch de Mixe Formation. During the post-rift stage, the scarps on the SMD and NMD detachments contributed a minor sedimentary flux while in the hyperextended domain, calcareous low-density turbidites originated from the European Upper Cretaceous carbonate platform.

Acknowledgments. This study was conducted within the framework of the integrated geological Orogen research project (TOTAL, BRGM, and INSU). We thank the Orogen project managers Sylvain Calassou (Total), Emmanuel Masini (Total), Olivier Vidal (CNRS) and Isabelle Thinon (French geological survey – BRGM). We thank Yves Lagabrielle for providing us the photos of the Urdach breccias in Figure 6. We specially thank Bulletin de la Société Géologique de France's deputy editor Olivier Lacombe and the three reviewers, Michel Séranne, Yohann Poprawski and Arantxa Bodego for their constructive comments, which significantly improved the initial manuscript.

References

Alhamawi M. 1992. Sédimentologie, pétrographie sédimentaire et diagenèse des calcaires du Cretacé supérieur de la Marge Ibérique. Bordeaux 1.

Alves TM, Cunha TA. 2018. A phase of transient subsidence, sediment bypass and deposition of regressive-transgressive cycles during the breakup of Iberia and Newfoundland. *Earth Planet. Sci. Lett.* 484: 168–183. https://doi.org/10.1016/j.epsl.2017.11.054.

Alves TM, Gawthorpe RL, Hunt DH, Monteiro JH. 2002. Jurassic tectono-sedimentary evolution of the Northern Lusitanian Basin (offshore Portugal). *Mar. Pet. Geol.* 19: 727–754. https://doi.org/10.1016/S0264-8172(02)00036-3.

Alves TM, Moita C, Sandnes F, Cunha T, Monteiro JH, Pinheiro LM. 2006. Mesozoic-Cenozoic evolution of North Atlantic continental slope basins: The Peniche Basin, Western Iberian margin. *AAPG Bull.* 90: 31–60. https://doi.org/10.1306/08110504138.

Alves TM, Moita C, Cunha T, Ullnaess M, Myklebust R, Monteiro JH, *et al.* 2009. Diachronous evolution of Late Jurassic-Cretaceous continental rifting in the northeast Atlantic (West Iberian margin). *Tectonics* 28. https://doi.org/10.1029/2008TC002337.

Alves TM, Fetter M, Busby C, Gontijo R, Cunha T, Mattos NH. 2020. A tectono-stratigraphic review of continental breakup on intraplate continental margins and its impact on resultant hydrocarbon systems. *Marine and Petroleum Geology* 117. https://doi.org/10.1016/j.marpetgeo.2020.104341.

Andrieu S, Saspiturry N, Lartigau M, Issautier B, Angrand P, Lasseur E. 2021. Large-scale vertical movements in Cenomanian to Santonian carbonate platform in Iberia: Indicators of a Coniacian

pre-orogenic compressive stress. *Bulletin de la Société Géologique de France*, Special Volume. https://doi.org/10.1051/bsgf/2021011.

Aslanian D, Moulin M, Olivet J-L, Unternehr P, Matias L, Bache F, *et al.* 2009. Brazilian and African passive margins of the Central Segment of the South Atlantic Ocean: Kinematic constraints. *Tectonophysics* 468: 98–112. https://doi.org/10.1016/j.tecto.2008.12.016.

Asti R, Lagabrielle Y, Fourcade S, Corre B, Monié P. 2019. How do continents deform during mantle exhumation? Insights from the Northern Iberia inverted paleopassive margin, Western Pyrenees (France). *Tectonics* 38: 1666–1693. https://doi.org/10.1029/2018TC005428.

Beltrando M, Manatschal G, Mohn G, Dal Piaz GV, Brovarone AV, Masini E. 2014. Recognizing remnants of magma-poor rifted margins in high-pressure orogenic belts: The Alpine case study. *Earth-Sci. Rev.* 131: 88–115.

Boillot G, Recq M, Winterer EL, Meyer AW, Applegate J, Baltuck M, *et al.* 1987. Tectonic denudation of the upper mantle along passive margins: A model based on drilling results (ODP leg 103, Western Galicia margin, Spain). *Tectonophysics* 132: 335–342.

Boillot G, Féraud G, Recq M, Girardeau J. 1989. Undercrusting by serpentinite beneath rifted margins: The example of the west Galicia margin (Spain). *Nature* 341: 523–525.

Boirie J-M. 1981. Étude sédimentologique des poudingues de Mendibelza (Pyrénées Atlantiques). Toulouse : Université Paul Sabatier de Toulouse (Sciences).

Boirie J-M, Souquet P. 1982. Les poudingues de Mendibelza : dépôts de cônes sous-marins du rift Albien des Pyrénées. *Bull. Cent. Rech. Explor. – Prod. Elf-Aquitaine* 6: 405–435.

Boissonnas J, Le Pochat G, Thibault C, Bernatzk M. 1974. Carte géologique de la France au 1/50 000 ; Feuille d'Iholdy, Orléans, France.

Bouma AH. 1962. Sedimentology of some flysch deposits. Elsevier, ed. Amsterdam: Elsevier Scientific Publishing Company.

Bouquet B. 1986. La bordure mésozoïque orientale du massif du Labourd (Pyrénées occidentales) : stratigraphie-sédimentologie-structure-implications géodynamiques. Pau : Université de Pau et des Pays de l'Adour.

Canérot J. 1988. Manifestations de l'halocinèse dans les chaînons béarnais (zone Nord-Pyrénéenne) au Crétacé inférieur. *C. R. Acad. Sci. Sér. 2 Mec. Phys. Chim. Sci. Univers Sci. Terre* 306: 1099–1102.

Canérot J. 1989. Rifting éocrétacé et halocinèse sur la marge ibérique des Pyrénées Occidentales (France). Conséquences structurales. *Bull. Cent. Rech. Explor. – Prod. Elf-Aquitaine* 13: 87–99.

Canérot J. 2008. Les Pyrénées : histoire géologique. Atlantica ed.

Canérot J. 2017. The pull apart-type Tardets-Mauléon Basin: A key to understand the formation of the Pyrenees. *Bull. Soc. geol. Fr.* 188: 35. https://doi.org/10.1051/bsgf/2017198.

Canérot J, Delavaux F. 1986. Tectonique et sédimentation sur la marge nord-ibérique des Chaînons Béarnais (Pyrénées-béarnaises). Remise en question de la signification des lherzolites du sommet de Saraillé. *C. R. Acad. Sci. Sér. 2 Mec. Phys. Chim. Sci. Univers Sci. Terre* 302: 951–956.

Canérot J, Lenoble J-L. 1993. Diapirisme crétacé sur la marge ibérique des Pyrénées occidentales ; exemple du pic de Lauriolle ; comparaisons avec l'Aquitaine, les Pyrénées centrales et orientales. *Bull. Soc. geol. Fr.* 164: 719–726.

Canérot J, Majesté-Menjoulas C, Ternet Y. 1999. Le cadre stratigraphique et géodynamique des altérites et des bauxites sur la marge ibérique des Pyrénées occidentales (France). *C. R. Acad. Sci. – Ser. IIA-Earth Planet. Sci.* 328: 451–456.

Canérot J, Hudec MR, Rockenbauch K. 2005. Mesozoic diapirism in the Pyrenean orogen: Salt tectonics on a transform plate boundary. *AAPG Bull.* 89: 211–229. https://doi.org/10.1306/09170404007.

Casteras M, Souquet P, Culot G, Galharague J. 1970. Carte géologique de la France au 1/50 000 ; Feuille de Larrau, Orléans, France.

Casteras M, Gottis M, Clin M, Guignard JD, Paris J, Galharague J. 1971. Carte géologique de la France au 1/50 000 ; Feuille de Tardets–Sorholus, Orléans, France.

Chevrot S, Sylvander M, Diaz J, Martin R, Mouthereau F, Manatschal G, *et al.* 2018. The non-cylindrical crustal architecture of the Pyrenees. *Sci. Rep.* 8: 9591. https://doi.org/10.1038/s41598-018-27889-x.

Claude D. 1990. Étude stratigraphique, sédimentologique et structurale des dépôts mésozoïques au nord du massif du Labourd : rôle de la faille de Pamplona (Pays Basque). Université de Bordeaux III.

Cochelin B, Chardon D, Denèle Y, Gumiaux C, Le Bayon B. 2017. Vertical strain partitioning in hot Variscan crust: Syn-convergence escape of the Pyrenees in the Iberian-Armorican syntax. *Bulletin de la Société Géologique de France* 188(6): 39. https://doi.org/10.1051/bsgf/2017206.

Contrucci I, Matias L, Moulin M, Géli L, Klingelhofer F, Nouzé H, *et al.* 2004. Deep structure of the West African continental margin (Congo, Zaïre, Angola), between 5 S and 8 S, from reflection/refraction seismics and gravity data. *Geophys. J. Int.* 158: 529–553.

Corre B, Lagabrielle Y, Labaume P, Fourcade S, Clerc C, Ballèvre M. 2016. Deformation associated with mantle exhumation in a distal, hot passive margin environment: New constraints from the Saraillé Massif (Chaînons Béarnais, North Pyrenean Zone). *Comptes Rendus Geosci.* 348: 279–289. https://doi.org/10.1016/j.crte.2015.11.007.

Curnelle R. 1983. Évolution structuro-sédimentaire du Trias et de l'Infra-Lias d'Aquitaine. *Bull. Cent. Rech. Explor. Prod. Elf-Aquitaine* 7: 69–99.

Daignières M, Séguret M, Specht M, Team ECORS. 1994. The Arzacq-Western Pyrenees ECORS deep seismic profile. In: *Hydrocarbon and Petroleum Geology of France*. Springer, pp. 199–208.

de Saint Blanquat M. 1993. La faille normale du massif du Saint-Barthélémy. Évolution hercynienne des massifs nord-pyrénéens catazonaux considérée du point de vue de leur histoire thermique. *Geodin Acta* 6: 59–77.

de Saint Blanquat M, Lardeaux JM, Brunel M. 1990, Petrological arguments for high temperature extensional deformation in the Pyrenean Variscan crust (Saint-Barthélémy Massif, Ariège, France).Tectonophysics 177: 245–262.

Debroas EJ. 1987. Modèle de bassin triangulaire à l'intersection de décrochements divergents pour le fossé albo-cénomanien de la Ballongue (Zone nord-pyrénéenne, France). *Bulletin de la Société géologique de France* 8(5): 887–898.

Debroas EJ. 1990. Le flysch noir albo-cénomanien témoin de la structuration albienne à sénonienne de la Zone nord-pyrénéenne en Bigorre (Hautes Pyrénées, Fr.). *Bulletin de la Société géologique de France* 8(6): 273–285.

Debroas EJ, Canérot J, Bilotte M. 2010. Les brèches d'Urdach, témoins de l'exhumation du manteau pyrénéen dans un escarpement de faille vraconnien-cénomanien inférieur (Zone nord-pyrénéenne, Pyrénées-Atlantiques, France). *Geol. Fr.* 2: 53–63.

Decarlis A, Manatschal G, Haupert I, Masini E. 2015. The tectono-stratigraphic evolution of distal, hyperextended magma-poor conjugate rifted margins: Examples from the Alpine Tethys and Newfoundland-Iberia. *Mar. Pet. Geol.* 68: 54–72. https://doi.org/10.1016/j.marpetgeo.2015.08.005.

DeFelipe I, Pedreira D, Pulgar JA, Iriarte E, Mendia M. 2017. Mantle exhumation and metamorphism in the Basque-Cantabrian Basin (NSpain): Stable and clumped isotope analysis in carbonates and comparison with ophicalcites in the North Pyrenean Zone

(Urdach and Lherz). *Geochem. Geophys. Geosyst.* 18: 631–652. https://doi.org/10.1002/2016GC006690.

Delaperrière E, de Saint Blanquat M, Brunel M, Lancelot J. 1994. Géochronologie U-Pb sur les zircons et monazites dans le massif du Saint-Barthélémy. *Bull. Soc. geol. Fr.* 2: 101–112.

Denèle Y, Laumonier B, Paquette JL, Olivier P, Gleizes G, Barbey P. 2014. Timing of granite emplacement, crustal flow and gneiss dome formation in the Variscan segment of the Pyrenees. *Geol. Soc. Spec. Publ.* 405: 265–287. https://doi.org/10.1144/SP405.5.

Driscoll NW, Hogg JR, Christie-Blick N, Karner GD. 1995. Extensional tectonics in the Jeanne d'Arc Basin, offshore Newfoundland: Implications for the timing of break-up between Grand Banks and Iberia. *Geol. Soc. Lond. Spec. Publ.* 90: 1–28. https://doi.org/10.1144/GSL.SP.1995.090.01.01.

Ducasse L, Velasque P-C. 1988. Géotraverse dans la partie occidentale des Pyrénées, de l'avant-pays aquitain au bassin de l'Ebre : effet d'une inversion structurale sur l'édification d'une chaîne intracontinentale. Aix-Marseille : Université Paul Cézanne, Faculté des sciences et techniques de Saint-Jérôme.

Duée G, Lagabrielle Y, Coutelle A, Fortané A. 1984. Les lherzolites associées aux Chaînons Béarnais (Pyrénées Occidentales) : mise à l'affleurement anté-dogger et resédimentation albo-cénomanienne. *C. R. Séances Acad. Sci. Sér. 2 Méc. Phys. Chim. Sci. Univers Sci. Terre* 299: 1205–1210.

Durand-Wackenheim C, Souquet P, Thiébaut G. 1981. La brèche d'Errozaté (Pyrénées-Atlantiques) : faciès de résedimentation en milieu profond de matériaux d'une plateforme carbonatée crétacée à substratum hercynien. *Bull. Soc. Hist. Nat. Toulouse* 117: 87–94.

Duretz T, Asti R, Lagabrielle Y, Brun J, Jourdon A, Clerc C, *et al.* 2019. Numerical modelling of Cretaceous Pyrenean rifting: The interaction between mantle exhumation and syn-rift salt tectonics. *Basin Res.* 32: 652–667. https://doi.org/10.1111/bre.12389.

Fabriès J, Lorand J-P, Bodinier JL, Dupuy C. 1991. Evolution of the Upper Mantle beneath the Pyrenees: Evidence from Orogenic Spinel Lherzolite Massifs. *Journal of Petrology, Special Volume* 2: 55–76. https://doi.org/10.1093/petrology/Special_Volume.2.55.

Fabriès J, Lorand J-P, Bodinier JL. 1998. Petrogenetic evolution of orogenic lherzolite massifs in the Central and Western Pyrenees. *Tectonophysics* 292: 145–167. https://doi.org/doi:10.1016/S0040-1951(98)00055-9.

Fixari G. 1984. Stratigraphie, faciès et dynamique tecto-sédimentaire du flysch albien (flysch noir et poudingues de mendibelza) dans la région de Mauléon-Tardets (Pyrénées Atlantiques). Université Paul Sabatier de Toulouse (Sciences).

Fortané A, Duée G, Lagabrielle Y, Coutelle A. 1986. Lherzolites and the western « Chaînons Béarnais » (French Pyrenees): Structural and paleogeographical pattern. *Tectonophysics* 129: 81–98. https://doi.org/10.1016/0040-1951(86)90247-7.

Frey M. 1968. Étude géologique de la partie occidentale et centrale du massif de Mendibelza (Basses Pyrénées). Toulouse.

Froitzheim N, Manatschal G. 1996. Kinematics of Jurassic rifting, mantle exhumation, and passive-margin formation in the Austro-alpine and Penninic nappes (Eastern Switzerland). *Geol. Soc. Am. Bull.* 108: 1120–1133. https://doi.org/10.1130/0016-7606(1996)108<1120:KOJRME>2.3.CO;2.

Garcia-Senz J, Pedrera A, Ayala C, Ruiz-Constán A, Robador Moreno A, Rodríguez-Fernández R. 2019. Inversion of the North Iberian hyperextended margin: The role of exhumed mantle indentation during continental collision. *Geological Society, London, Special Publications* 490. https://doi.org/10.1144/SP490-2019-112.

Gómez-Romeu J, Masini E, Tugend J, Ducoux M, Kusznir N. 2019. Role of rift structural inheritance in orogeny highlighted by the Western Pyrenees case study. *Tectonophysics* 766: 131–150. https://doi.org/10.1016/j.tecto.2019.05.022.

Gubler Y, Casteras M, Ciry R, Lamare P. 1947. Sur l'âge des poudingues dits de Mendibelza dans le bassin du Laurhibar, au SE de Mendive (Basse Pyrénées). *C. R. Soc. Geol. Fr.* 17: 329–330.

Hart NR, Stockli DF, Hayman NW. 2016. Provenance evolution during progressive rifting and hyperextension using bedrock and detrital zircon U-Pb geochronology, Mauléon Basin, Western Pyrenees. *Geosphere* 12: 1166–1186. https://doi.org/10.1130/GES01273.1.

Hart NR, Stockli DF, Lavier LL, Hayman NW. 2017. Thermal evolution of a hyperextended rift basin, Mauléon Basin, Western Pyrenees: Thermal evolution of hyperextended rift. *Tectonics*. https://doi.org/10.1002/2016TC004365.

Haupert I, Manatschal G, Decarlis A, Unternehr P. 2016. Upper-plate magma-poor rifted margins: Stratigraphic architecture and structural evolution. *Mar. Pet. Geol.* 69: 241–261. https://doi.org/10.1016/j.marpetgeo.2015.10.020.

Issautier B, Saspiturry N, Serrano O. 2020. Role of structural inheritance and salt tectonics in the formation of pseudosymmetric continental rifts on the european margin of the hyperextended Mauléon Basin (Early Cretaceous Arzacq and Tartas Basins). *Mar. Pet. Geol.* 118: 104395. https://doi.org/10.1016/j.marpetgeo.2020.104395.

James V. 1998. La plate-forme carbonatée ouest-pyrénéenne au jurassique moyen et supérieur stratigraphie séquentielle, stades d'évolution, relations avec la subsurface en aquitaine méridionale.

James V, Canérot J. 1999. Diapirisme et structuration post-triasique des Pyrénées occidentales et de l'Aquitaine méridionale (France). *Eclogae Geol. Helvetiae* 92: 63–72.

Jammes S, Manatschal G, Lavier L, Masini E. 2009. Tectono-sedimentary evolution related to extreme crustal thinning ahead of a propagating ocean: Example of the Western Pyrenees. *Tectonics* 28. https://doi.org/10.1029/2008TC002406.

Johnson JA, Hall CA. 1989. Tectono-stratigraphic model for the Massif D'Igountze-Mendibelza, Western Pyrenees. *J. Geol. Soc.* 146: 925–932. https://doi.org/10.1144/gsjgs.146.6.0925.

Karner GD, Gambôa LAP. 2007. Timing and origin of the South Atlantic pre-salt sag basins and their capping evaporites. *Geol. Soc. Lond. Spec. Publ.* 285: 15–35. https://doi.org/10.1144/SP285.2.

Karner GD, Driscoll NW, Barker DHN. 2003. Syn-rift regional subsidence across the West African continental margin: The role of lower plate ductile extension. *Geol. Soc. Lond. Spec. Publ.* 207: 105–129. https://doi.org/10.1144/GSL.SP2003.207.6.

Labaume P, Teixell A. 2020. Evolution of salt structures of the Pyrenean Rift (Chaînons Béarnais, France): From hyperextension to tectonic inversion. *Tectonophysics* 785: 228451. https://doi.org/10.1016/j.tecto.2020.228451.

Lagabrielle Y, Bodinier J-L. 2008. Submarine reworking of exhumed sub-continental mantle rocks: Field evidence from the Lherz peridotites, French Pyrenees: Cretaceous exhumation of pyrenean mantle. *Terra Nova* 20: 11–21. https://doi.org/10.1111/j.1365-3121.2007.00781.x.

Lagabrielle Y, Labaume P, de Saint Blanquat M. 2010. Mantle exhumation, crustal denudation, and gravity tectonics during Cretaceous rifting in the Pyrenean realm (SW Europe): Insights from the geological setting of the lherzolite bodies. *Tectonics* 29. https://doi.org/10.1029/2009TC002588.

Lagabrielle Y, Asti R, Fourcade S, Corre B, Poujol M, Uzel J, *et al.* 2019. Mantle exhumation at magma-poor passive continental margins. Part I. 3D architecture and metasomatic evolution of a fossil exhumed mantle domain (Urdach lherzolite, northwestern Pyrenees, France). *BSGF – Earth Sci. Bull.* 190: 8. https://doi.org/10.1051/bsgf/2019007.

Lagabrielle Y, Asti R, Duretz T, Clerc C, Fourcade S, Teixell A, *et al.* 2020. A review of cretaceous smooth-slopes extensional basins along the Iberia-Eurasia plate boundary: How pre-rift salt controls the modes of continental rifting and mantle exhumation. *Earth-Sci. Rev.* 201: 103071. https://doi.org/10.1016/j.earscirev.2019.103071.

Lamare P. 1946. Les formations détritiques crétacées du massif de Mendibelza. *Bull. Soc. geol. Fr.* 16: 265–312.

Lamare P. 1948. Sur le passage latéral des faciès détritiques grossiers du Crétacé du massif de Mendibelza aux faciès schisto-gréseux classiques de l'Albien des Pyrénées. *C. R. Acad. Sci.* 226: 683–685.

Lowe DR. 1982. Sediment gravity flows: II. Depositional models with special reference to the deposits of high-density turbidity currents. *Journal of Sedimentary Petrology* 52(I): 279–297.

Le Pochat G, Bolthenhagen C, Lenguin M, Lorsignol S, Thibault C. 1976. Carte géologique de France au 1/50 000 : Mauléon-licharre, Orléans, France.

Le Pochat G, Heddebaut C, Lenguin M, Lorsignol S, Souquet P, Muller J, *et al.* 1978. Carte géologique de France au 1/50 000 : St Jean Pied de Port, Orléans, France.

Leleu S, Hartley AJ, van Oosterhout C, Kennan L, Ruckwied K, Gerdes K. 2016. Structural, stratigraphic and sedimentological characterisation of a wide rift system: The Triassic Rift system of the Central Atlantic Domain. *Earth-Sci. Rev.* 158: 89–124.

Lemirre B. 2018. Origine et développement de la thermicité dans les Pyrénées varisques. PhD Thesis, Univ. Paul Sabatier, Toulouse, France, 299 p.

Lemoine M, Tricart P, Boillot G. 1987. Ultramafic and gabbroic ocean floor of the Ligurian Tethys (Alps, Corsica, Apennines): In search of a genetic imodel. *Geology* 15: 622–625. https://doi.org/10.1130/0091-7613(1987)15<622:UAGOFO>2.0.CO;2.

Lenoble J-L. 1992. Les plates-formes carbonatées ouest-pyrénéennes du dogger à l'Albien, stratigraphie séquentielle et évolution géodynamique. Université Paul Sabatier de Toulouse (Sciences).

Lescoutre R, Manatschal G. 2020. Role of rift-inheritance and segmentation for orogenic evolution: Example from the Pyrenean-Cantabrian system. *BSGF – Earth Sci. Bull.* 191: 18. https://doi.org/10.1051/bsgf/2020021.

Lescoutre R, Tugend J, Brune S, Masini E, Manatschal G. 2019. Thermal evolution of asymmetric hyperextended magma-poor rift systems: Results from numerical modeling and Pyrenean field observations. *Geochem. Geophys. Geosyst.* 20: 4567–4587. https://doi.org/10.1029/2019GC008600.

Lescoutre R, Manatschal G, Muñoz J-A. 2021. Nature, origin and evolution of the Pyrenean-Cantabrian junction. *Tectonics.* https://doi.org/10.1029/2020TC006134.

Lucas C. 1985. Le grès rouge du versant nord des Pyrénées : essai sur la géodynamique de dépôts continentaux du permien et du trias.

Magné. 1948. Nouvelles observations relatives à l'âge des poudingues du pic Errozaté (massif de Mendibelza). *C. R. Soc. Geol. Fr.* 163–165.

Manatschal G, Nievergelt P. 1997. A continent-ocean transition recorded in the Err and Platta nappes (Eastern Switzerland). *Eclogae Geol. Helvetiae* 90: 3–28.

Manatschal G, Froitzheim N, Rubenach M, Turrin BD. 2001. The role of detachment faulting in the formation of an ocean-continent transition: Insights from the Iberia Abyssal Plain. *Geol. Soc. Lond. Spec. Publ.* 187: 405–428. https://doi.org/10.1144/GSL.SP2001.187.01.20.

Manatschal G, Engström A, Desmurs L, Schaltegger U, Cosca M, Müntener O, *et al.* 2006. What is the tectono-metamorphic evolution of continental break-up: The example of the Tasna Ocean-Continent Transition. *J. Struct. Geol.* 28: 1849–1869. https://doi.org/10.1016/j.jsg.2006.07.014.

Manatschal G, Sauter D, Karpoff AM, Masini E, Mohn G, Lagabrielle Y. 2011. The Chenaillet Ophiolite in the French/Italian Alps: An ancient analogue for an oceanic core complex? *Lithos* 124: 169–184. https://doi.org/10.1016/j.lithos.2010.10.017.

Martín-Chivelet J, Berástegui X, Rosales I, Vilas L, Vera JA, Caus E, *et al.* 2002. Cretaceous. In: Gibbons W, Moreno T, ed. *The Geology of Spain*, pp. 255–292.

Masini E, Manatschal G, Mohn G, Ghienne J-F, Lafont F. 2011. The tectono-sedimentary evolution of a supra-detachment rift basin at a deep-water magma-poor rifted margin: The example of the Samedan Basin preserved in the Err nappe in SE Switzerland: Tectono-sedimentary evolution of a supra-detachment rift basin. *Basin Res.* 23: 652–677. https://doi.org/10.1111/j.1365-2117.2011.00509.x.

Masini E, Manatschal G, Mohn G, Unternehr P. 2012. Anatomy and tectono-sedimentary evolution of a rift-related detachment system: The example of the Err detachment (Central Alps, SE Switzerland). *Geol. Soc. Am. Bull.* 124: 1535–1551. https://doi.org/10.1130/B30557.1.

Masini E, Manatschal G, Tugend J, Mohn G, Flament J-M. 2014. The tectono-sedimentary evolution of a hyperextended rift basin: The example of the Arzacq-Mauléon Rift system (Western Pyrenees, SW France). *Int. J. Earth Sci.* 103: 1569–1596. https://doi.org/10.1007/s00531-014-1023-8.

Merle J-M. 1974. Recherches sur les relations paléogéographiques et structurales entre les massifs basques au sud de Saint-Jean-Pied-de-Port (Pyrénées occidentales). Université Paul Sabatier de Toulouse (Sciences).

Mirouse R. 1967. Le Dévonien des Pyrénées occidentales et centrales (France). *Int. Symp. Devonian Syst.* I: 153–170.

Moulin M, Aslanian D, Unternehr P. 2010. A new starting point for the South and Equatorial Atlantic Ocean. *Earth-Sci. Rev.* 98: 1–37. https://doi.org/10.1016/j.earscirev.2009.08.001.

Muller J, Roger P. 1977. L'évolution structurale des Pyrénées (Domaine central et occidental) Le segment hercynien, la chaîne de fond alpine. *Geol. Alp.* 53: 149–191.

Mutti E. 1977. Distinctive thin-bedded turbidite facies and related depositional environments in the Eocene Hecho Group (South-central Pyrenees, Spain). *Sedimentology* 24: 107–131.

Mutti E. 1992. Turbidite sandstones. AGIP, Istituto di geologia, Università di Parma.

Olivet JL. 1996. La cinématique de la plaque ibérique. *Bull. Cent. Rech. Explor. Prod. Elf Aquitaine* 20: 131–195.

Pedrera A, García-Senz J, Ayala C, Ruiz-Constán A, Rodríguez-Fernández LR, Robador A *et al.* 2017. Reconstruction of the exhumed mantle across the North Iberian Margin by crustal-scale 3-D gravity inversion and geological cross section. *Tectonics* 36: 3155–3177.

Pedrera A, García-Senz J, Peropadre C, Robador A, Lopez Mir B, Diaz Alvarado J, *et al.* 2020. The Getxo crustal-scale cross-section: Testing tectonic models in the Bay of Biscay-Pyrenean Rift system. *Earth-Sciences Review.* https://doi.org/10.1016/j.earscirev.2020.103429.

Pérez-Gussinyé M. 2013. A tectonic model for hyperextension at magma-poor rifted margins: An example from the West Iberia-Newfoundland conjugate margins. *Geol. Soc. Lond. Spec. Publ.* 369: 403–427. https://doi.org/10.1144/SP369.19.

Péron-Pinvidic G, Manatschal G. 2009. The final rifting evolution at deep magma-poor passive margins from Iberia-Newfoundland: A new point of view. *Int. J. Earth Sci.* 98: 1581–1597. https://doi.org/10.1007/s00531-008-0337-9.

Péron-Pinvidic G, Manatschal G, Minshull TA, Sawyer DS. 2007. Tectonosedimentary evolution of the deep Iberia-Newfoundland

margins: Evidence for a complex breakup history. *Tectonics* 26: 1–19. https://doi.org/10.1029/2006TC001970.

Péron-Pinvidic G, Manatschal G, Osmundsen PT. 2013. Structural comparison of archetypal Atlantic rifted margins: A review of observations and concepts. *Mar. Pet. Geol.* 43: 21–47. https://doi.org/10.1016/j.marpetgeo.2013.02.002.

Péron-Pinvidic G, Manatschal G, Masini E, Sutra E, Flament JM, Haupert I, *et al.* 2015. Unravelling the along-strike variability of the Angola-Gabon rifted margin: A mapping approach. *Geol. Soc. Lond. Spec. Publ.* 438: 49–76. https://doi.org/10.1144/SP438.1.

Péron-Pinvidic G, Manatschal G, The "IMAGinING RIFTING" Workshop Participants. 2019. Rifted margins: State of the art and future challenges. *Front. Earth Sci.* 7: 218. https://doi.org/10.3389/feart.2019.00218.

Peybernès B. 1976. Le Jurassique et le Crétace inferieur des Pyrénées franco-espagnoles entre la Garonne et la Méditérranée. Toulouse.

Poprawski Y. 2012. La marge Nord du Fossé Basque à l'Albien : architecture sédimentaire et diapirisme dans un contexte décrochant (Pays Basque, Espagne). PhD Thesis, Grenoble University.

Puigdefàbregas C, Souquet P. 1986. Tecto-sedimentary cycles and depositional sequences of the Mesozoic and Tertiary from the Pyrenees. *Tectonophysics* 129: 173–203.

Razin P. 1989. Évolution tecto-sédimentaire alpine des Pyrénées basques à l'ouest de la transformante de Pamplona, Province du Labourd. Bordeaux 3.

Reston TJ. 2009. The structure, evolution and symmetry of the magma-poor rifted margins of the North and Central Atlantic: A synthesis. *Tectonophysics* 468: 6–27. https://doi.org/10.1016/j.tecto.2008.09.002.

Ribes C, Ghienne J-F, Manatschal G, Decarlis A, Karner GD, Figueredo PH, *et al.* 2019. Long-lived mega fault-scarps and related breccias at distal rifted margins: Insights from present-day and fossil analogues. *J. Geol. Soc.* 176: 801–816.

Richard P. 1986. Structure et évolution alpine des massifs paléozoïques du Labourd (Pays Basque français). Éditions du Bureau de recherches géologiques et minières.

Rossi P, Cocherie A, Fanning CM, Ternet Y. 2003. Datation U-Pb sur zircons des dolérites tholéiitiques pyrénéennes (igneous rockss) à la limite Trias-Jurassique et relations avec les tufs volcaniques dits « infra-liasiques » nord-pyrénéens. *Comptes Rendus Geosci.* 335: 1071–1080. https://doi.org/10.1016/j.crte.2003.09.011.

Rossy M, Azambre B, Albarède F. 1992. REE and Sr/1bNd isotope geochemistry of the alkaline magmatism from the Cretaceous North Pyrenean Rift Zone (France-Spain). *Chem. Geol.* 97: 33–46. https://doi.org/10.1016/0009-2541(92)90134-Q.

Roux J-C. 1983. Recherches stratigraphiques et sédimentologiques sur les flyschs crétacés pyrénéens au sud d'Oloron (Pyrénées Atlantiques). Université Paul Sabatier de Toulouse (Sciences).

Saspiturry N. 2019. Évolution sédimentaire, structurale et thermique d'un rift hyper-aminci : de l'héritage post-hercynien à l'inversion alpine : exemple du bassin de Mauléon (Pyrénées). PhD Thesis, Bordeaux 3.

Saspiturry N, Cochelin B, Razin P, Leleu S, Lemirre B, Bouscary C, *et al.* 2019a. Tectono-sedimentary evolution of a rift system controlled by Permian post-orogenic extension and metamorphic core complex formation (Bidarray Basin and Ursuya dome, Western Pyrenees). *Tectonophysics* 768: 228180. https://doi.org/10.1016/j.tecto.2019.228180.

Saspiturry N, Razin P, Baudin T, Serrano O, Issautier B, Lasseur E, *et al.* 2019b. Symmetry vs. asymmetry of a hyper-thinned rift: Example of the Mauléon Basin (Western Pyrenees, France). *Mar. Pet. Geol.* 104: 86–105. https://doi.org/10.1016/j.marpetgeo.2019.03.031.

Saspiturry N, Allanic C, Razin P, Issautier B, Baudin T, Lasseur E, *et al.* 2020a. Closure of a hyperextended system in an orogenic lithospheric pop-up, Western Pyrenees: The role of mantle buttressing and rift structural inheritance. *Terra Nova* 32: 253–260. https://doi.org/10.1111/ter.12457.

Saspiturry N, Lahfid A, Baudin T, Guillou-Frottier L, Razin P, Issautier B, *et al.* 2020b. Paleogeothermal gradients across an inverted hyperextended rift system: Example of the Mauléon Fossil Rift (Western Pyrenees). *Tectonics* 39. https://doi.org/10.1029/2020TC006206.

Saspiturry N, Issautier B, Razin P, Baudin T, Asti R, Lagabrielle Y, *et al.* 2021. Review of Iberia-Eurasia plate-boundary basins: Role of sedimentary burial and salt tectonics during rifting and continental breakup. *Basin Res.* bre.12529. https://doi.org/10.1111/bre.12529.

Souquet P. 1967. Le Crétacé supérieur Sud-Pyrénéen, en Catalogne, Aragon et Navarre. E. Privat.

Souquet P, Bilotte M, Canérot J, Debroas E, Peybernés B, Rey J. 1975. Nouvelle interprétation de la structure des Pyrénées. *C. R. Acad. Sci. Paris* 281: 609–612.

Souquet P, Peybènes B, Bilotte M, Debroas E-J. 1977. La chaîne alpine des Pyrénées. *Geol. Alp.* 53: 193–216.

Souquet P, Debroas E-J, Boirie J-M, Pons P, Fixari G, Roux J-C, *et al.* 1985. Le groupe du Flysch noir (albo-cénomanien) dans les Pyrénées. *Bull. Cent. Rech. Explor.-Prod. Elf-Aquitaine Pau* 9: 183–252.

Teixell A. 1998. Crustal structure and orogenic material budget in the west Central Pyrenees. *Tectonics* 17: 395–406. https://doi.org/10.1029/98TC00561.

Teixell A, Labaume P, Lagabrielle Y. 2016. The crustal evolution of the west-central Pyrenees revisited: Inferences from a new kinematic scenario. *C. R. Geosci.* 348: 257–267. https://doi.org/10.1016/j.crte.2015.10.010.

Teixell A, Labaume P, Ayarza P, Espurt N, de Saint Blanquat M, Lagabrielle Y. 2018. Crustal structure and evolution of the Pyrenean-Cantabrian Belt: A review and new interpretations from recent concepts and data. *Tectonophysics* 724-725: 146–170. https://doi.org/10.1016/j.tecto.2018.01.009.

Ternet Y, Majesté-Menjoulas C, Canérot J, Baudin T, Cocherie A, Guerrot C, *et al.* 2004. Carte géologique de la France au 1/50 000 : Laruns-Somport, Orléans, France.

Tugend J, Manatschal G, Kusznir NJ. 2015. Spatial and temporal evolution of hyperextended rift systems: Implication for the nature, kinematics, and timing of the Iberian-European plate boundary. *Geology* 43: 15–18. https://doi.org/10.1130/G36072.1.

Tugend J, Gillard M, Manatschal G, Nirrengarten M, Harkin C, Epin M-E, *et al.* 2018. Reappraisal of the magma-rich versus magma-poor rifted margin archetypes. *Geol. Soc. Lond. Spec. Publ.* SP476.9. https://doi.org/10.1144/SP476.9.

Unternehr P, Péron-Pinvidic G, Manatschal G, Sutra E. 2010. Hyperextended crust in the South Atlantic: in search of a model. *Pet. Geosci.* 16: 207–215. https://doi.org/10.1144/1354-079309-904.

Vacherat A, Mouthereau F, Pik R, Huyghe D, Paquette J-L, Christophoul F, *et al.* 2017. Rift-to-collision sediment routing in the Pyrenees: A synthesis from sedimentological, geochronological and kinematic constraints. *Earth-Sci. Rev.* 172: 43–74.

Vielzeuf D. 1984. Relations de phases dans le faciès granulite et implications géodynamiques: l'exemple des granulites des Pyrénées. Université Clermont-Ferrand II.

Vielzeuf D, Paquette J-L, Clemens J-D, Stevens G, Gannoun A, Suchorski K, *et al.* 2021. Age, duration and mineral markers of magma interactions in the deep crust: An example from the Pyrenees. *Contrib. Miner. Pet.* 176: 39. https://doi.org/10.1007/s00410-021-01789-2.

Wang Y, Chevrot S, Monteiller V, Komatitsch D, Mouthereau F, Manatschal G, *et al.* 2016. The deep roots of the Western Pyrenees revealed by full waveform inversion of teleseismic P-waves. *Geology* 44: 475–478. https://doi.org/10.1130/G37812.1.

Cite this article as: Saspiturry N, Issautier B, Razin P, Andrieu S, Lasseur E, Allanic C, Serrano O, Baudin T, Cochelin B. 2021. Review of the syn-rift to early post-rift depositional systems of the Cretaceous Mauléon rift: sedimentary record of continental crust hyperextension and mantle denudation (Western Pyrenees), *BSGF - Earth Sciences Bulletin* 192: 49.